DESIGN AND FABRICATION OF A FLUIDIZED BED REACTOR FOR HEMATITE REDUCTION

By

B. V. KUMAR

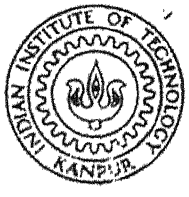

DEPARTMENT OF METALLURGICAL ENGINEERING

INDIAN INSTITUTE OF TECHNOLOGY KANPUR

AUGUST, 1984

DESIGN AND FABRICATON OF A FLUIDIZED BED REACTOR FOR HEMATITE REDUCTION

A Thesis Submitted
in Partial Fulfilment of the Requirements
for the Degree of

MASTER OF TECHNOLOGY

By

B. V. KUMAR

to the

DEPARTMENT OF METALLURGICAL ENGINEERING

INDIAN INSTITUTE OF TECHNOLOGY KANPUR

AUGUST, 1984

CERTIFICATE

This is to certify that the thesis entitled, "DESIGN AND FABRICATION OF A FLUIDIZED BED REACTOR FOR HEMATITE REDUCTION" by Mr. B.V. Kumar has been carried out under my supervision, and this has not been submitted elsewhere for a degree.

(Dr. S.P. Mehrotra)
Assistant Professor
Department of Metallurgical Engineering
I.I.T. Kanpur

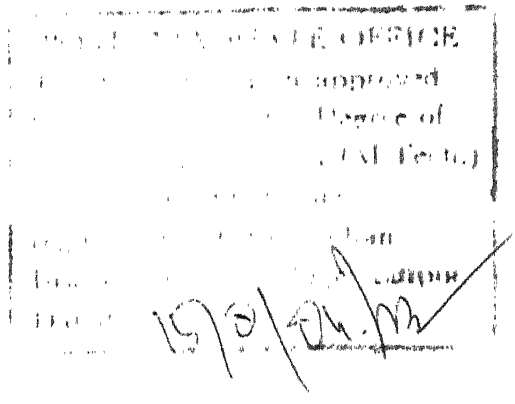

ACKNOWLEDGEMENT

I would like to express my profound gratitude to Dr. S.P. Mehrotra for his guidance and encouragement during the course of execution of the project.

I am grateful to Dr. N.K. Batra for his variety of assistance during my stay here.

I am deeply indebted to Devesh Goyal and Sanjeev Saxena who involved themselves in shaping this thesis.

I should sincerely acknowledge the timely help from my friends, Mr. D. Ramakrishna, Mr. G. Babu-viswanathan, Mr. Deepak Goyal and Mr. R.S. Mishra, who directly or indirectly involved in the preparation of this thesis.

I am highly thankful to Mr. D.P. Tripathi & Mr. A. Sharma whose efforts helped me in the successful execution of the project.

I sincerely acknowledge Mr. S.J. Gupta of Aeronautical Engineering Department for his neat and faultless typing.

B. V. Kumar

ABSTRACT

A high temperature fluidized bed reactor (FBR) was designed and fabricated to study high temperature endothermi gas-solid reactions, in particular, the reduction of hematit with solid, solid and gas, and gaseous reductants. The design of this FBR was based on extensive studies carried out on a cold model FBR made of perspex through which the fluidization behaviour could be visually observed.

The physical dimensions of the room temperature FBR were more or less identical to those used for high temperature FBR. Three different distributor plate designs were examined and the one that gave the most uniform fluidization behaviour for a larger range of operating variables was chosen for the actual high temperature FBR.

The experimental part in this study has been divided into two sections. First section deals with the design and fabrication of the cold model fluidized bed reactor. A large number of experiments were carried out using this reactor to study the fluidization characteristics for different operating variables namely, the type of materials, particle size, bed height etc. Visual observations and analyses of pressure drop versus velocity plots were used as the main criterion for establishing the optimum conditions for fluidization.

The second section deals with the design and fabrication of high temperature FBR and its auxiliaries such as preheater, methane gas generator etc. A few experiments on reduction of hematite with coke, and hydrogen were carried out to establish the workability of the high temperature FBR. Originally planned experiments on reduction of hematite with coke and methane had to be abandoned because of the problems with the chromatograph which made the online analysis of the outgoing gases impossible.

TABLE OF CONTENTS

CHAPTER - 1

INTRODUCTION

Fluidisation is a process in which the solid particles are rendered fluid when they come in contact with a flowing fluid. The process was discovered late in the eighteenth century and was commercially adopted for various industrial processes as early as the beginning of this century. Fluidization can be regarded as the most effective method of fluid-solid contact.

In extractive metallurgy, the fluidized bed reactors are used for various gas-solid reactions such as roasting, reduction, calcination, chlorination, etc. The applications of fluidization in the field of Hydrometallurgy and Electro-metallurgy are the subjects of recent research investigations. However since most of the extractive metallurgical processes which use the fluidized bed i.e. involve gas-solid reaction we shall confine our discussion to fluidized bed reactors involving gas solid only.

1.1 A FLUIDIZED BED REACTOR (FBR)

An FBR consists of a long cylinder, at the bottom of which is provided a distributor plate which has large number of pores/holes. The solids used are taken in the form of uniformly sized powder, and the gas is passed through the solid bed at a sufficiently high flow rate, which fluidizes the solids.

The reactor may be made of stainless steel, glass, plastic, etc. depending on various factors such as application, type of study, temp. of operation, nature of gaseous environment present, etc.

1.2 PHENOMENON OF FLUIDIZATION

When gas is passed through a bed of solid particles, four distinct stages are observed at different flow rates of fluids.

At low flow rates, the gas permeates through the bed of solid particles without displacing them. This stage is termed as "Fixed bed". The pressure drop across the bed is proportional to the gas velocity.

When the flow rate is continued to increase, a state is reached at which the weight of the bed and the frictional forces between the solids and the fluid are exactly equal to the drag force due to the flowing gas. This point corresponds to the maximum pressure drop across the bed.

Further increase in flow rate results in the "Expanded bed". In this stage, the bed begins to expand with gas velocity and the pressure drop remains almost constant.

When the flow rate is continued to increase further, a stage is reached at which there is no expansion in the bed and the particles in the bed start behaving like a boiling liquid. This is marked by a drop in the pressure drop across the bed, and remains almost constant with the increase in gas

velocity. This stage is termed as "Turbulent stage" or "incipiently fluidized" stage. The last stage, namely "pneumatic transport" stage is reached. Gas velocity is equal to the value of terminal velocity of particles. Here the particles are physically carried along with the fluid.

1.3 MERITS & DEMERITS OF A FBR

MERITS

1. The smooth, liquid like flow of particles allows continuous, automatically controlled operations with ease of handling.
2. Rapid mixing of solids leads to nearly isothermal conditions in the reactor.
3. Heat and mass transfer between the particles are high as compared to other modes of contacting.
4. The residence time of particles can be controlled.
5. By choosing proper fluidization conditions, it is possible to maintain the gas composition very close to the equilibrium conditions.

DEMERITS

1. Segregation and entrainment of the particles can occur above the surface of fluidized bed.
2. It is not possible to control the reaction of individual particle. It is only the average fraction reacted that can be controlled.

1.4 APPLICATIONS OF FLUIDIZATION IN EXTRACTIVE METALLURGY

The major gas-solid reactions, such as roasting, reduction calcination, chlorination etc. are extensively carried out using FBR. The research investigations in the field of sulfide roasting of common metals in FBR are mainly on the kinetic aspects of the oxidation of sulfide in FBR (4-8). The reduction of non-ferrous oxides in FBR using gaseous reducing agents has started getting more and more attention recently (9,10). The investigation on selective chlorination & separation of Titaniferrous minerals in FBR have also been reported in literature (11,12).

Besides these, FBRs are also finding commercial applications in gassification of coal (13), Calcination of lime and dolomite (14).

Recently, applications of FBR with reasonable success in hydro-metallurgical & Electrometallurgical processes have also been reported (2).

1.5 PRESENT STUDY

The present study is on the fluidized bed reduction of hematite ore using gaseous reducing agent. For this purpose, a high temperature FBR has been designed and fabricated. The design and fabrication of the reactor are based on the theoretical as well as the cold-model studies, which are discussed in the subsequent chapters.

CHAPTER - 2

THEORETICAL ASPECTS OF FBR DESIGN

The process of fluidization is one of the most important modes of solid-gas contact. The theoretical treatment of the subject is of utmost importance from the point of view of design and is presented in this chapter.

2.1 PRESSURE DROP ACROSS THE BED

The pressure drop across the fixed bed of uniformly sized particles is given by Ergun (1,3)

$$\frac{\Delta P}{L} \cdot g_c = 150 \frac{(1-\epsilon_m)^2}{\epsilon_m^3} \frac{\mu u_o}{(\phi_s d_p)^2} + 1.75 \frac{(1-\epsilon_m)\rho_g u_o^2}{\epsilon_m^3 (\phi_s d_p)} \quad \ldots (2.1$$

Where, P = pressure drop across the bed

L = Length of the bed

ϵ_m = Porosity of the bed

d_p = particle size

ϕ_s = Shape factor

ρ_g = gas density

μ = gas viscosity

u_o = superficial gas velocity

This equation represents two important factors influencing the pressure drop across the bed, namely, the viscous and the kinetic energy factors. At low Reynolds No., ($Re_p < 20$), the viscous forces predominate, hence simplification of Eq. (2.1) results in

$$\frac{\Delta P}{L} g_c = 150 \frac{(1-\epsilon_m)^2}{\epsilon_m^3} \frac{\mu u_o}{(\phi_s d_p)^2} \; ; Re_p < 20 \quad \ldots \quad \ldots \quad (2.2)$$

At high Reynolds No., (Re> 1000), the kinetic energy losses predominates, modifying the Ergun equation to

$$\frac{\Delta P}{L} g_c = 1.75 \frac{(1-\epsilon_m)\rho_p u_o^2}{\epsilon_m^2 (\phi_s d_p)} ; Re_p > 1000 \quad \ldots (2.3)$$

At Reynolds No., 20 < Rep < 1000, Eq. (2.1) is used. A Schematic pl of Δ P-V relationship is illustrated in Fig. 2.1.

The onset of fluidization occurs when the drag force of gas is equal to the weight of the bed. i.e.,

$$\left(\begin{matrix}\text{Pressure drop} \\ \text{across bed}\end{matrix}\right)\left(\begin{matrix}\text{Cross-sectional} \\ \text{area of tube}\end{matrix}\right) =$$

$$\left(\begin{matrix}\text{Volume} \\ \text{of bed}\end{matrix}\right)\left(\begin{matrix}\text{fraction} \\ \text{of solids}\end{matrix}\right)\left(\begin{matrix}\text{specific weight} \\ \text{of solids}\end{matrix}\right) \quad \ldots (2.4)$$

Mathematically

$$\Delta P . A_t = W = (A_t . L_{mf})(1-\epsilon_{mf})\left[(\rho_s - \rho_g)\frac{g}{g_c}\right] \quad \ldots (2.5)$$

Rearranging the terms,

$$\frac{\Delta P}{L_{mf}} = (1 - \epsilon_{mf})(\rho_s - \rho_g)\frac{g}{g_c} \quad \ldots (2.6)$$

2.2 MINIMUM FLUIDIZATION VELOCITY (u_{mf}) (1,16,17)

Minimum fluidization velocity can be defined as that minimum fluid velocity which just renders the fixed bed fluidized.

The following is the theoretical prediction of minimum fluidization velocity using the parameters such as particle size, particle density, gas viscosity, porosity etc.

Combining Eq. (2.6) with Eq. (2.1) and using Eq. (2.2) or Eq.(2.3) (depending on the Reynolds number), the superficial velocity at minimum fluidization conditions is given by

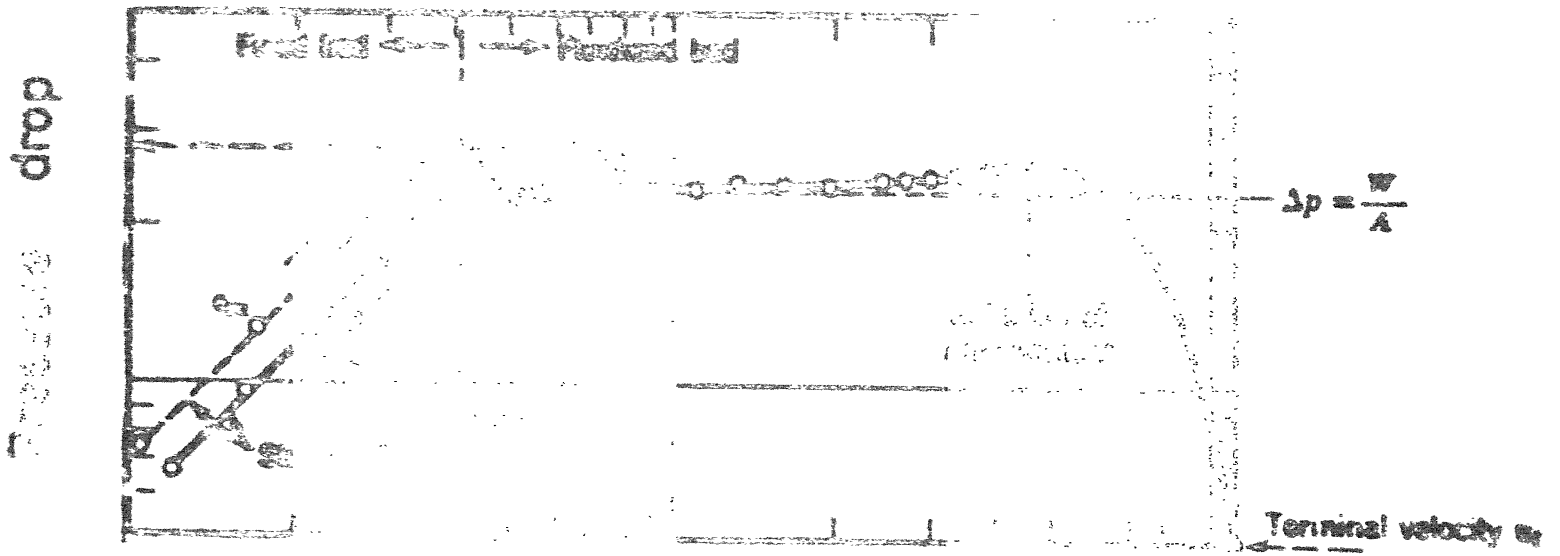

Fig. 2.1. Pressure drop vs gas velocity for a bed of uniform sized particles.

$$u_{mf} = \frac{(\phi_s d_p)^2}{150} \left(\frac{\rho_s - \rho_g}{\mu}\right) . g . \left(\frac{\epsilon_{mf}^3}{1-\epsilon_{mf}}\right) ; \; Re_p < 20 \; .. \qquad (2.7)$$

or

$$u_{mf}^2 = \frac{(\phi_s d_p)}{1.75} \left(\frac{\rho_s - \rho_g}{\rho_g}\right) . g . \epsilon_{mf}^3 \; ; \; Re_p > 1000 \; .. \qquad (2.8)$$

If ϵ_{mf} and/or ϕ_s are unknown the following empirical equations may be used (1).

$$\frac{1}{\phi_s \, \epsilon_{mf}^3} \simeq 14 \qquad .. \qquad (2.9)$$

$$\frac{1 - \epsilon_{mf}}{\phi_s^2 \, \epsilon_{mf}^3} \simeq 11 \qquad .. \qquad (2.10)$$

Using Eq. (2.9) and Eq. (2.10) in Eqns. (2.1), (2.7) and (2.8) the equations for minimum fludization velocity for different Reynolds No. can be obtained.

$$u_{mf} = \left[\left(\frac{33.7\,\mu}{g\,d_p}\right)^2 + 0.0408 \, \frac{d_p(\rho_s - \rho_g)}{\rho_g} \, g\right]^{1/2} - \frac{33.7\,\mu}{d_p \rho_g} \qquad .. \qquad (2.11)$$

$$u_{mf} = \frac{d_p^2 \, (\rho_s - \rho_g) g}{1650\,\mu} \; ; \; Re_p < 20 \qquad .. \qquad (2.12)$$

$$u_{mf}^2 = \frac{d_p(\rho_s - \rho_g)}{24.5\,\rho_g} \; ; \; Re_p > 1000 \qquad .. \qquad (2.13)$$

2.3 TERMINAL VELOCITY (u_t) (1,3,17):

The upper limit to gas flow rate above u_{mf} is the terminal velocity u_t. The terminal velocity can be expressed in terms of drag co-efficient C_d as follows.

$$u_t = \left[\frac{4\,g\,d_p(\rho_s - \rho_g)}{3\,\rho_g\,C_d}\right]^{1/2} \qquad .. \qquad (2.14)$$

For both spherical and non-spherical particles, the terminal velocity u_t can be obtained from an experimental correlation $C_d\ Re_p^2$ vs Re_p plot (Appendix I) (1)

where

$$C_d\ Re_p^2 = \frac{4 g\ d_p^3 \rho_g\ (\rho_s - \rho_g)}{3\ \mu^2} \quad \ldots \quad (2.15)$$

u_t can be determined by determining $C_d\ Re_p^2$ knowing dp, ρ_s, ρ_g and μ. From this corresponding Re_p, hence u_t can be calculated.

The gas flow rate through an FBR is limited by two quantities, u_{mf} on one hand and u_t on the other. These two are most important factors which influence the design of an FBR. To avoid carryover the solids from an FBR, the velocity of gas should be $u_{mf} < u_{op} < u_t$.

2.4 DESIGN CONSIDERATIONS (1,14,19)

The design of a fluidized bed reactor depends on the factors such as type of solids handled, size of particles and the amount to be handled. Knowing these, the diameter of the FBR can be calculated. This diameter is limited by the capacity of pumps and availability of gaseous phase.

Distributor design (19)

The most important design parameter is the design of distributor. This is because the distributor influences the quality of fluidization to the greatest extent than any other parameter. This is exemplified in fig. 2.2. It is experimentally established that, larger the number of pores/ holes in distributor, better will be the quality of fluidization.

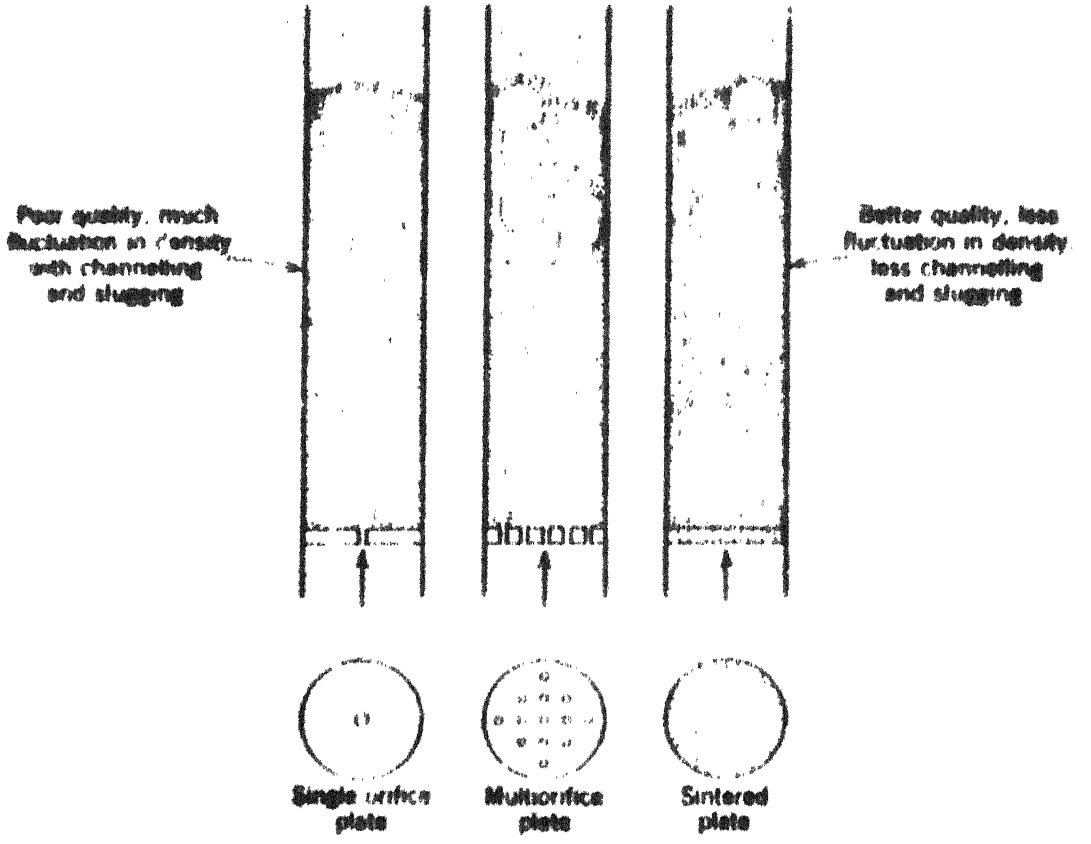

Fig.2.2. Quality of Fluidization as influenced by type of gas distributor.

For industrial FBRs, a wide variety of distributor designs are available. Some of them are shown in Fig. 2.3. Of these, type (a) and (b) are most commonly used in the laboratory investigations of FBR.

It is important to note that the distributors should have a sufficiently high pressure drop in order to achieve equal flow through the openings. It has been experimentally deduced that the pressure drop across the distributor plate should roughly be 10 percent of the pressure drop across the bed (1,19).

$$P_{d,min} = \text{Max.} \left[0.1 \quad P_{bed} \right] \qquad .. \qquad (2.16)$$

For a fixed, maximum bed height, P_{bed} can be calculated from the Eq. (2.2) or Eq. (2.3) and hence P_d is evaluated from Eq. (2.16). Once the superficial velocity (u_o) of the gas is known it is possible to calculate the Reynolds number which then can be used to calculate C_d' from the C_d' vs Re plot given in Appendix II (1).

Knowing C_d' , the velocity of gas through the orifice (u_{or}) can be calculated using the following Eq. (2.17).

$$u_{or} = C_d' \left(\frac{2g_c \cdot P_d}{g}\right)^{1/2} \qquad .. \qquad (2.17)$$

Knowing u_{or}, N_{or}, the number of pores per unit area of distributor plate can be evaluated from the equation

$$\frac{u_o}{u_{or}} = \frac{\pi}{4} d_{or}^2 \; N_{or} \qquad .. \qquad (2.18)$$

2.5 OTHER DESIGN PARAMETERS(1,3,14,16,17,19):

Besides the distributor design the other design parameters include the diameter of the reactor and its

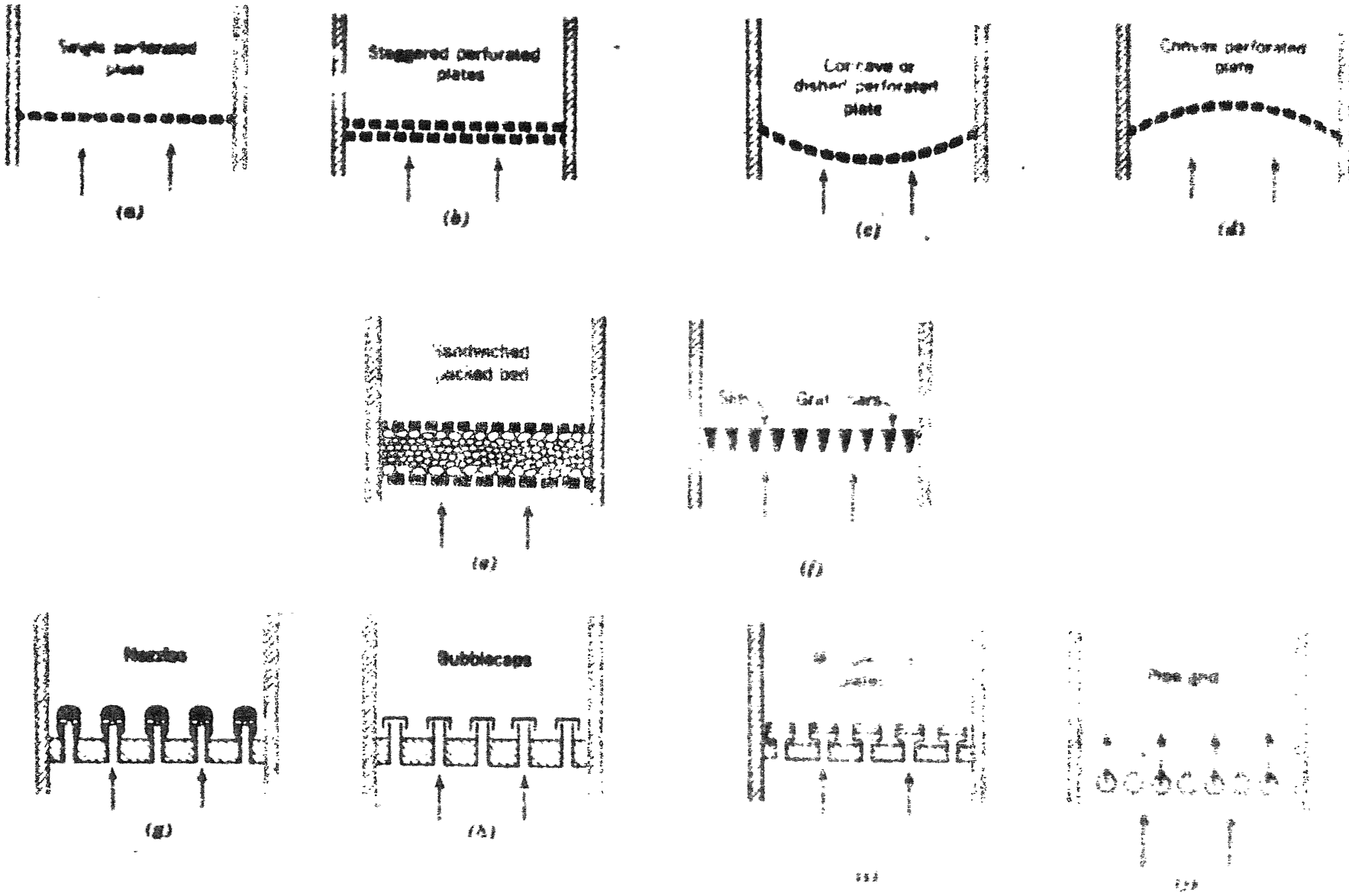

Fig. 2.3. Types of Distributor Plates

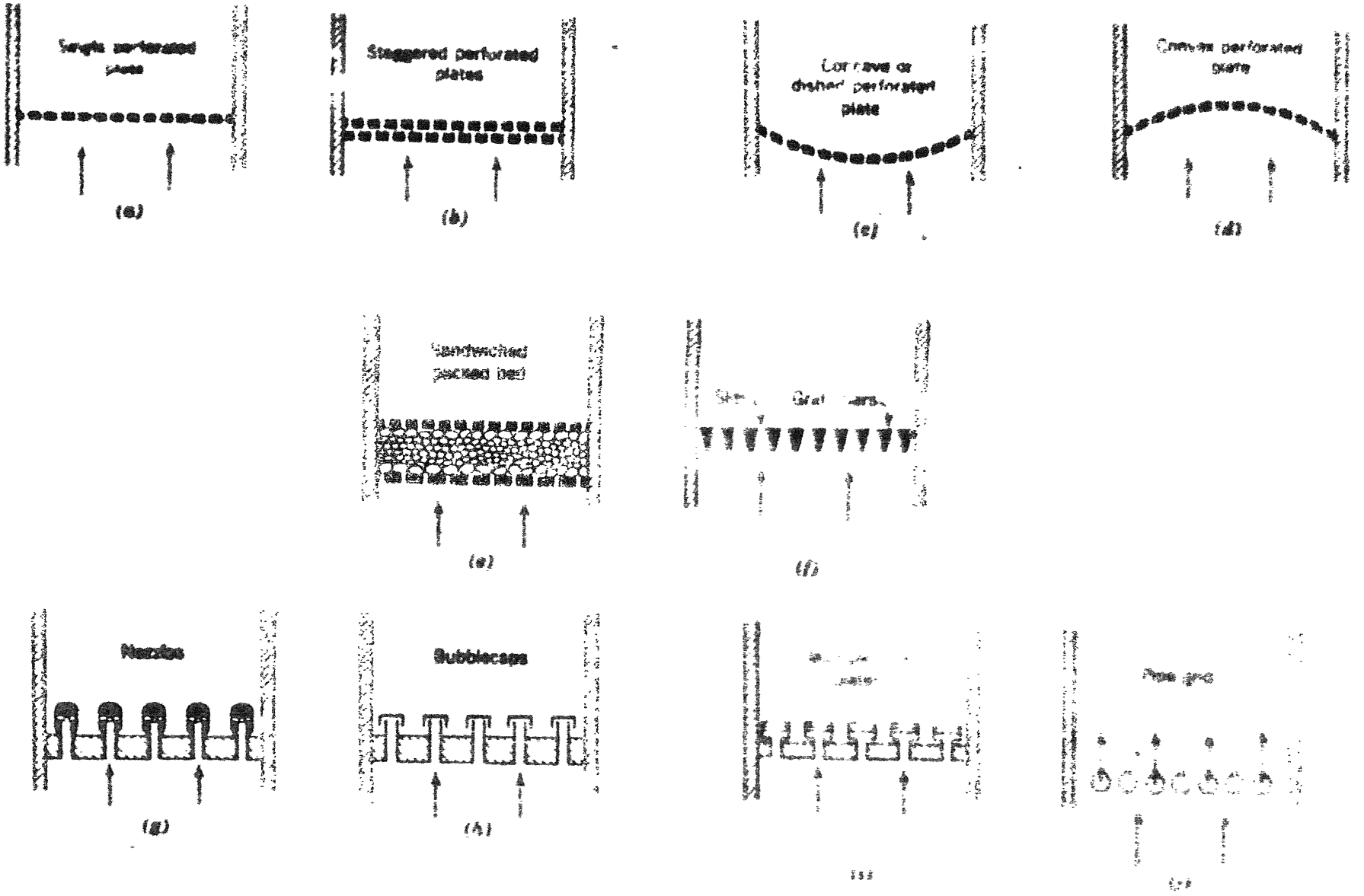

Fig. 2.3. Types of Distributor Plates

height, selection of construction material for the reactor and design of the preheater depends on the parameters like the type of application, temperature at which the reaction is carried out etc.

2.6 PROBLEMS ENCOUNTERED IN FBR (1,2,3,14)

At this point, it would be desirable to mention some of the common problems that one encounters in a FBR either due to the faulty design of the reactor or due to undesirable operating conditions. These are channelling and slugging. The pressure drop vs velocity plots for these two are schematically shown in Figs. 2.4 (a) and (b).

Channelling : Channelling in fluidized bed occurs when the pores in the distributor plate are too large or when there is sticking of particles at some parts of the bed. This also occurs when the particle size are not uniform.

Slugging : It occurs when the bed is too long due to the coalescence of bubbles forming a large bubble, of the size of the reactor itself. The Δ P- Velocity diagrams of fluidized beds are very helpful when the fluidization phenomenon cannot be observed visually, in a reactor. Many a times it is possible to recognise a fault, if it exists, by looking at these diagrams.

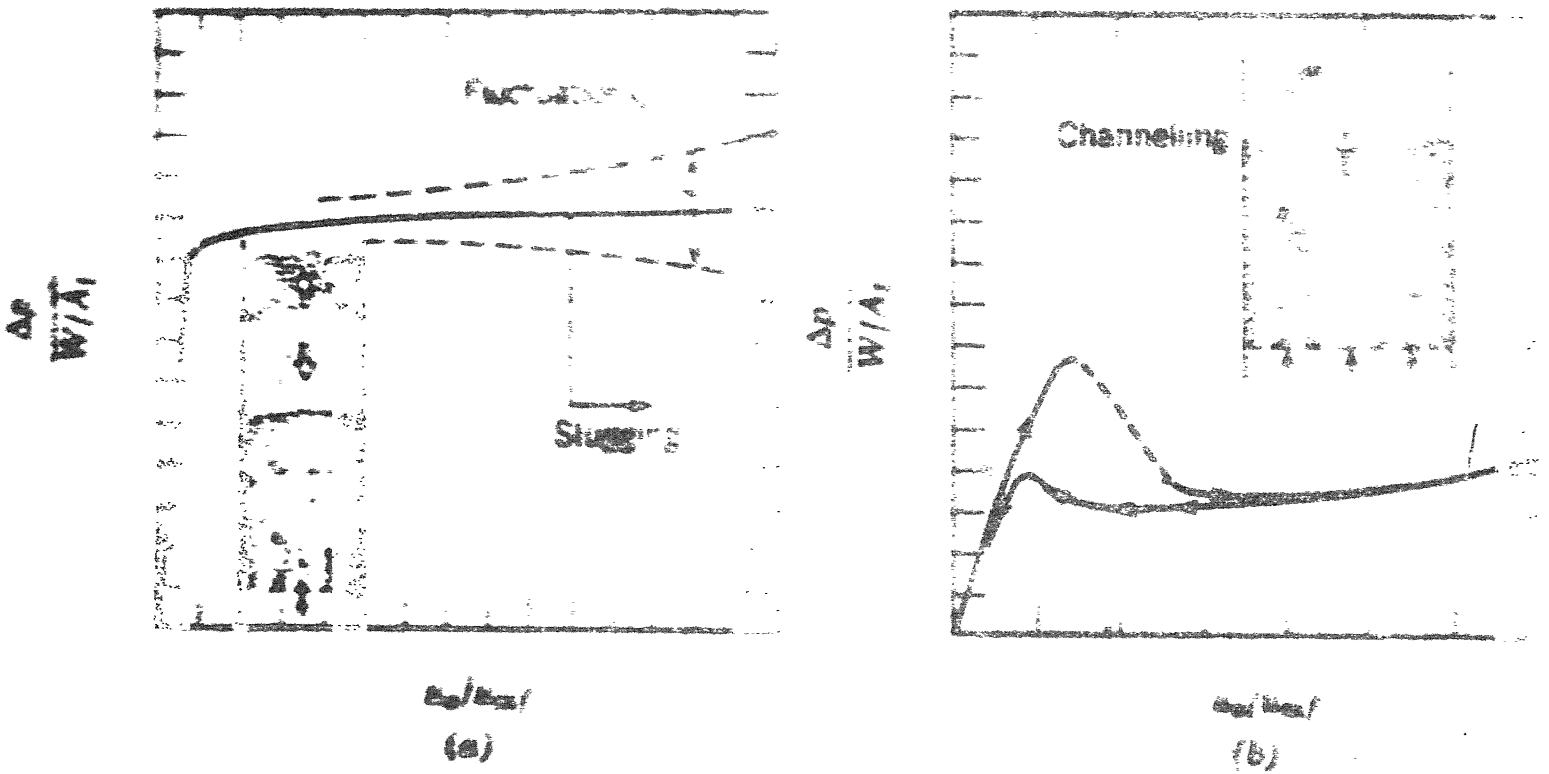

Fig.2.4. Pressure drop diagrams for poorly fluidised bed.

CHAPTER 3

OBJECTIVE OF THE PRESENT STUDY

The present study was intended to explore the reduction of Hematite fines using gaseous as well as solid reducing agents in Fluidized Bed Reactor (FBR). As there was no ready-made FBR available for this purpose, the task of designing and fabricating an FBR was undertaken.

It was considered desirable to design and fabricate a cold model before going for the design and fabrication of the high temp. FBR. The main advantage of cold model is that the visual observation of the fluidization and the related phenomenon is possible.

The present investigation can be divided into three distinct parts.

In the first part a room temp. FBR was designed and fabricated and the effects of parameters such as particle-size, particle density, bed height, distributor design, etc. were studied.

Using the design parameters of the cold model FBR, a high temp. FBR was designed and fabricated in the second part of the work. Though for many components of this reactor, the same design criterion was used as for the cold model FBR, it was found necessary to change some of the design parameters. The reasons for these changes are discussed in details in one of the following chapters.

The main objective of the third part of this study was to study the various aspects of reduction of hematite with coke and with coke and methane, using nitrogen as the fluidizing gas. It is known that the rate of reduction of hematite is much higher with methane as compared to that with coke. It is also known that using methane as the only reducing agent is not economical particularly in countries like ours where it is not available in abundance. It was therefore hoped to find out the optimum conditions for reduction of hematite with coke and methane simultaneously and, thus, suggest a new method for sponge iron production. However, this project had to be abandoned due to the malfunctions of the chromatograph which was to be used for the on line analysis of the outgoing gases to determine the extent of reduction as a function of time. Therefore, the third part of this investigation was finally reduced to a few set of experiments to test the workability of the high temp. FBR. The reduction experiments carried out for this purpose involved.

(i) reduction of hematite with coke using nitrogen as fluidizing gas and

(ii) reduction of hematite with hydrogen using nitrogen and hydrogen gas mixture as the fluidizing gas.

For the purpose of presentation the next three chapters have been divided in two sections. The first section

deals with the study using the cold model FBR where as the design and fabrication of the high temperature FBR, and reduction of Hematite in this reaction are presented in Section II.

CHAPTER - 4

COLD MODEL STUDIES

This chapter deals with the design and fabrication of cold model fluidized bed reactor. A number of experiments were carried out using this reactor to arrive at the optimum design of the high temperature FBR and also to establish the optimum conditions for fluidization of different variables. The results of these experiments are presented and discussed in this chapter.

4.1 DESIGN AND FABRICATION OF COLD MODEL FBR

A detailed discussion on the theoretical aspects on the design of FBR has been given in chapter 2. In this investigation, it was proposed to design a FBR in which study on the reduction of hematite fines was intended. So the particle size, the particle density and the amount of material used will constitute the primary factors for design. From these preliminary data and from the available blower capacity, an optimum diameter of 5 cms was arrived at.

The length of the reactor is governed by TDH as well as entrainment allowances. Since in the laboratory models, furnace allowance also must be taken into account, reactor height of 60 cms was chosen.

Perspex was chosen as the construction material for the cold model. It was preferred to glass because it is non-fragile and easily machinable.

The design of distributor plate is the most important part of the FBR design. To design a distributor plate, approximate value of the pressure drop of the bed should be known. This can be calculated using factors such as particle size, density and bed height. Assuming a bed height of 10 cms, the open area and pore size were calculated. For the present investigation, an open area of 1.3% was found necessary.

A distributor with 1.3% open area may be a porous sintered plate or a perforated plate. Since in the latter case, a large number of perforations is not possible, it will adversely affect the fluidization characteristics. As it could not be possible to acquire sintered porous plate, it was decided to fabricate a perforated plate having an open area of 3.59% . This would help in having a reasonable number of pores (40 in number) of diameter 1/16". In order to compensate loss in pressure drop due to the larger area of distributor plate, two 325 mesh sieves were cut to the dimensions of the distributor plate and placed above it. This would help in formation of small bubbles in the fluidized bed also. Three different distributor plates of same open area but different hole configuration were fabricated. They are as shown in Fig. 4.1.

The details of the cold model FBR is illustrated in Fig. 4.2. Two side tubes were provided above and below the distributor plate to measure the pressure drop across the bed.

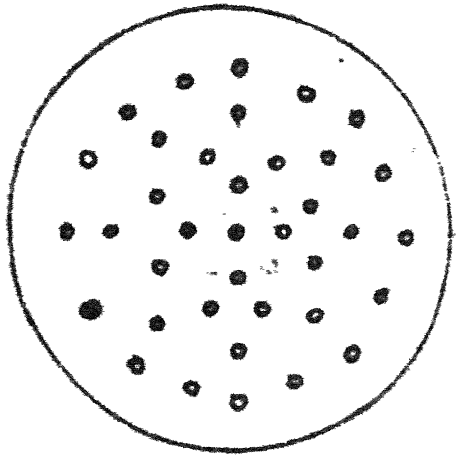

D_1

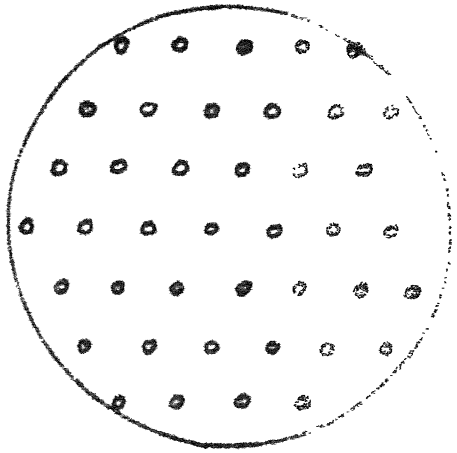

D_2

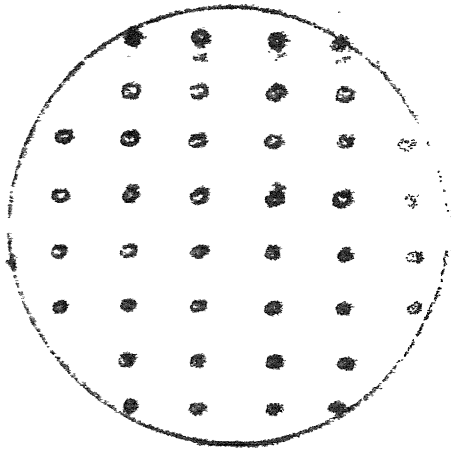

D_3

Fig. 4.1. Configuration of pores in Distributor plates. (Schematic)

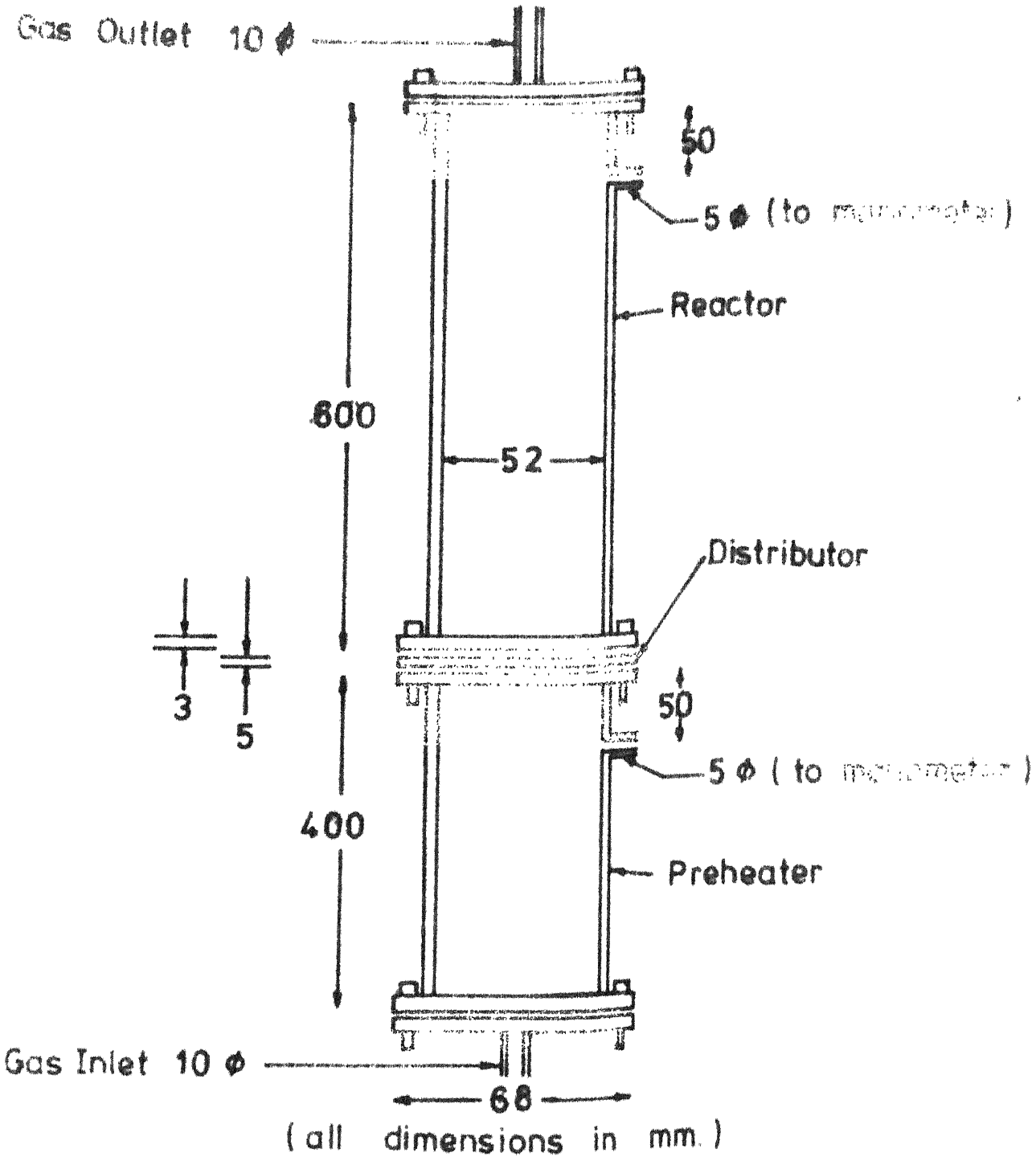

Fig. 4.2. Cold model FBR details

The preheater just below the distributor was filled with glass marbles as it will be done in the preheater of high temperature FBR.

A number of experiments were carried out using this cold model and are described and discussed in the following section.

4.2 EXPERIMENTAL PROCEDURE

A number of experiments were carried out to study the fluidization characteristics of the FBR. The main variables whose effect on fluidization behaviour were examined included distributor design, type of materials, bed height and particle size.

The experimental conditions employed in various experiments are tabulated in Table No. 4.1 and Table No.4.2.

The cold model experimental set up is as shown in Fig. 4.3. In a typical experiment uniformly sized material was charged in the FBR from the top, so as to form a bed of certain height. The air from the compressor is passed through the reactor, at a very low gas velocity, to begin with. The gas velocity was slowly increased and the pressure drop in cms of H_2O was measured as a function of gas velocity. Before noting the pressure drop in the manometer, sufficient time was allowed for bed to stabilise each time after the gas velocity was changed. The results of the cold mode experiments are presented and discussed below.

4.3 RESULTS AND DISCUSSION

Variation of pressure drop with gas velocity constituted the main experimental data. Visual observation of the bed

Table No.4.1 Expdrimental Conditions Employed In Cold Model Experimen

S.No.	Material used (d_1=Hematiate	Distributor type	Particle size in mesh	Bed Height (in cm.)	Combination
1.	d_1	D_1	P_1-72+100	2	$D_1P_1H_1d_1$
				4	$D_1P_1H_2d_1$
				6	$D_1P_1H_3d_1$
			P_2-100 +150	2	$D_1P_2H_1d_1$
				4	$D_1P_2H_3d_1$
				6	$D_1P_2H_3d_1$
			P_3-150+170	2	$D_1P_3H_1d_1$
				4	$D_1P_3H_2d_1$
				6	$D_1P_3H_3d_1$
2.	d_1	D_2	P_1-72+100	2	$D_2P_1H_1d_1$
				4	$D_2P_1H_2d_1$
				6	$D_2P_1H_3d_1$
			P_2-100+150	2	$D_2P_2H_1d_1$
				4	$D_2P_2H_2d_1$
				6	$D_2P_2H_2d_1$
			P_3-150+170	2	$D_2P_3H_1d_1$
				4	$D_2P_3H_2d_1$
				6	$D_2P_3H_3d_1$
3.	d_1	D_3	P_1-72+100	2	$D_3P_1H_1d_1$
				4	$D_3P_1H_2d_1$
				6	$D_3P_1H_3d_1$
			P_2-100+150	2	$D_3P_2H_1d_1$
				4	$D_3P_2H_2d_1$
				6	$D_3P_2H_3d_1$
			P_3-150+170	2	$D_3P_3H_1d_1$

Table No.4.2 Experimental Conditions Employed in Cold Model Ex

Sl.No.	Material used (d_2=sand)	Distributor type	Particle size in mesh	Bed height (in cms.) H_1=2, H_2=4, H_3=6	Combinat
1.	d_2	D_1	P_1:-72+100	2	$D_1P_1H_1d_2$
				4	$D_1P_1H_2d_2$
				6	$D_1P_1H_3d_2$
			P_2:-100+150	2	$D_1P_2H_1d_2$
				4	$D_1P_2H_2d_d$
				6	$D_1P_2H_3d_2$
			P_3:-150+170	2	$D_1P_3H_1d_2$
				4	$D_1P_3H_2d_2$
				6	$D_1P_3H_3d_2$
2.	d_2	D_2	P_1:-72+100	2	$D_2P_1H_1d_2$
				4	$D_2P_1H_2d_2$
				6	$D_2P_1H_3d_2$
			P_2:-100+150	2	$D_2P_2H_1d_2$
				4	$D_2P_2H_2d_2$
				6	$D_2P_1H_3d_2$
			P_3:-150+170	2	$D_2P_3H_1d_2$
				4	$D_2P_3H_2d_2$
				6	$D_2P_3H_3d_2$
3.	d_2	D_3	P_1:-72+100	2	$D_3P_1H_1d_2$
				4	$D_3P_1H_2d_2$
				6	$D_3P_1H_3d_2$
			P_2:-100+150	2	$D_3P_2H_1d_2$
				4	$D_3P_2H_2d_2$
				6	$D_3P_2H_3d_2$
			P_3:-150+170	2	$D_3P_3H_1d_2$
				4	$D_3P_3H_2d_2$
				6	$D_3P_3H_3d_2$

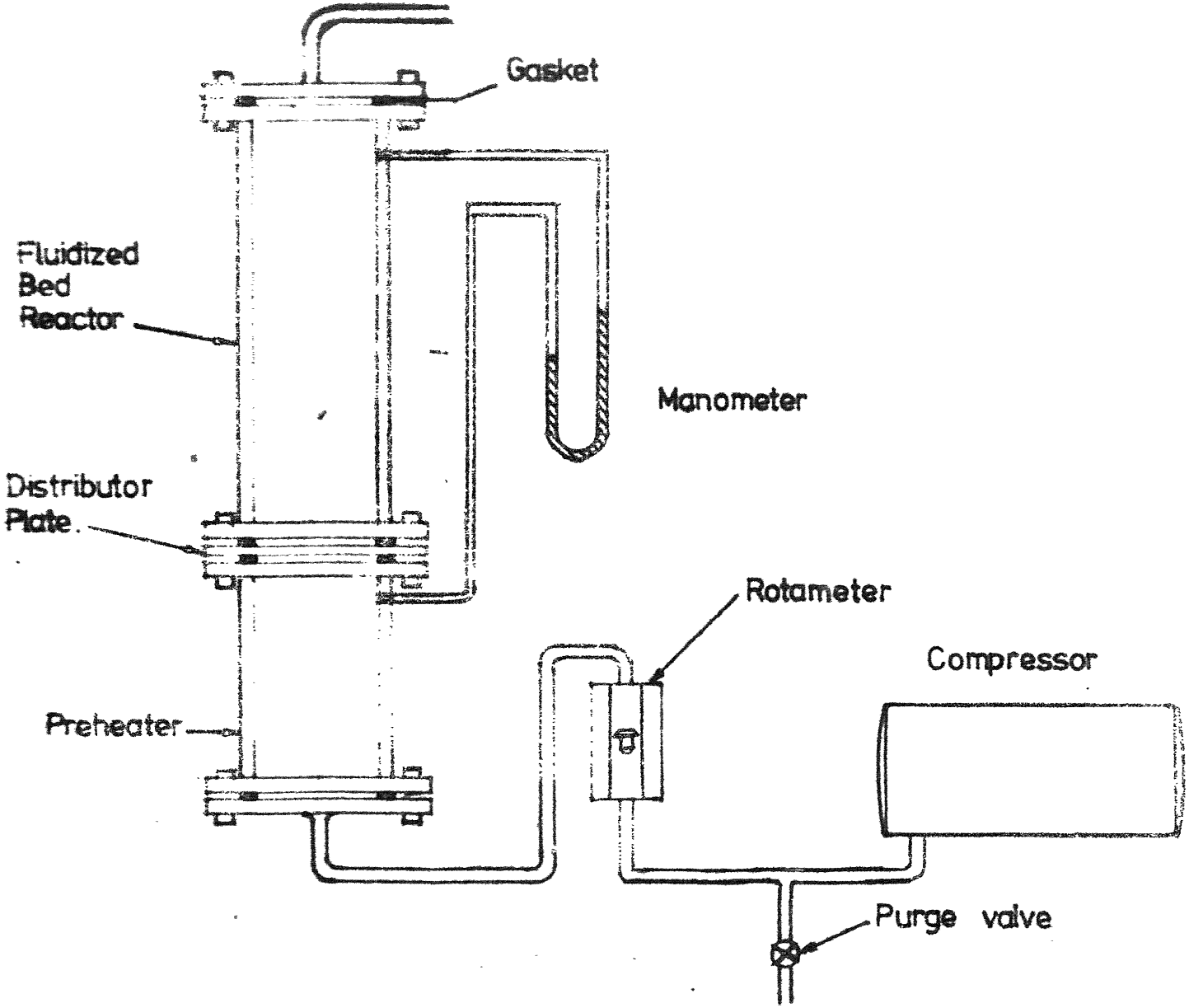

Fig.4.3. Cold Model Fluidised Bed Reactor - Experimental set-up

behaviour were recorded to verify the quantitative prediction of fluidization behaviour using the pressure-drop velocity relationships.

The variation of pressure drop with gas velocity for the various experiments including visual observations are tabulated in Tables 4.3-4.8. The corresponding ΔP vs ga velocity are presented in Figs. 4.5-4.22.

The comparison of the experimental and theoretical values of the pressure drop across the bed and minimum fluidiz velocity are tabulated in Tables 4.9-4.10.

EFFECT OF DISTRIBUTOR PLATE(19):

A close inspection of the ΔP-velocity plots of cold model experiments and its comparison with the typical plot in Fig. 2.4 coupled with the visual observation, leads to the division of all the experimental results into two categories with respect to the quality of fluidizati The plots in Fig. 4.5-4.10, which correspond to the distributor D_1, exhibit normal fluidization conditions whereas those in Figs. 4.11-4.16 corresponding to the distributor D_2 and Figs. 4.17-4.22 corresponding to the distributor D_3 are poorly fluidized.

Channelling was visually observed at some parts of the bed in D_2 and D_3, for finer particle sizes. It was more severe at larger bed heights.

Table No. 4.3 : Experimental Observations in Cold Model FBR

S.No.	$D_1P_1H_1d_1$			$D_1P_1H_2d_1$			$D_1P_1H_3d_1$		
	V (cm/sec.)	P (cm of H_2O)	Visual obs.	V (cm/sec.)	P (cm of H_2O)	Visual obs.	V (cm/sec.)	P (cm of H_2O)	Visual obs.
1.	0.70	1.8		0.95	3.4		0.40	2.4	
2.	0.97	2.6		1.45	4.8		0.75	4.8	
3.	1.07	2.8	F.B.	1.75	5.8	F.B.	1.15	6.8	F.B.
4.	1.25	2.9		1.90	6.6		1.60	9.6	
5.	1.17	3.4		2.00	7.0		1.75	11.0	
6.	1.20	3.6		2.10	7.4		1.80	12.0	
7.	1.30	3.8		2.35	6.4		1.90	12.2	
8.	1.57	3.8		2.40	6.0		1.95	11.6	
9.	1.60	3.4	Fl.B	2.45	6.2	Fl.B	2.20	10.6	Fl.B
10	1.62	3.2		2.75	6.2		2.40	10.0	
11.	1.95	3.0		3.15	6.4		2.45	10.0	
		$D_1P_2H_1d_1$			$D_1P_1H_2d_1$			$D_1P_2H_3d_1$	
	[illegible]	2.0		0.32	2.8		0.30	4.0	
2.	0.47	2.4		0.50	4.0		0.45	5.8	
3.	0.62	3.4		0.72	5.8		0.55	6.6	
4.	0.70	3.6	F.B	0.80	6.2	F.B	0.80	10.6	F.B
5.	0.75	4.0		0.90	7.6		0.90	12.4	
6.	0.80	4.2		0.95	8.0		0.95	12.8	
7.	0.97	2.8		1.25	7.2		1.30	11.4	
8.	1.02	2.6	Fl.B	1.30	6.8	Fl.B	1.40	11.6	Fl.B
9.	1.22	2.8		1.35	6.2		1.90	11.4	
10.	1.72	2.8		1.95	6.2		2.50	11.4	
11.	1.90	3.2		2.20	6.2		3.05	11.2	
		$D_1P_3H_1d_1$			$D_1P_3H_2d_1$			$D_1P_3H_3d_1$	
1.	0.25	2.0		0.35	[illegible]		[illegible]	4.8	
2.	0.30	2.8		0.55	7.0		0.35	9.0	
3.	0.35	3.2	F.B	0.65	8.4	F.B	0.60	10.8	F.B
4.	0.40	3.6		0.70	8.0		0.65	11.4	
5.	0.45	4.2		0.95	7.6		0.70	12.4	
6.	0.65	3.0		1.05	7.2		0.75	13.0	
7.	0.70	3.2		1.25	7.4		[illegible]	12.6	
8.	0.72	3.0	Fl.B	1.65	7.4	Fl.B	1.10	12.0	Fl.B
9.	1.15	3.2		2.00	7.6		1.50	11.8	
10.	1.55	3.4		2.50	7.8		2.15	12.0	
11.	1.90	3.2		2.52	7.8		2.70	12.0	

Table No.4.4 Experimental Observations in Cold Model F B R

S.No.	$D_1P_1H_1d_2$ V (cm/sec)	$D_1P_1H_1d_2$ P H_2Ocm	Visual obs.	$D_1P_1H_2d_2$ V (cm/Sec.)	$D_1P_1H_2d_2$ P H_2Ocm	Visual obs.	$D_1P_1H_3d_2$ V (cm./sec)	$D_1P_1H_3d_2$ P H_2Ocm	Vis obs
1.	0.50	0.3		0.30	1.4		0.35	1.9	
2.	0.75	0.8	FB	0.75	1.5	FB	0.60	1.7	Fl.
3.	0.90	1.2		0.90	1.9		0.75	2.2	
4.	1.13	1.8		1.13	2.3		1.20	2.9	
5.	1.25	1.3		1.25	2.6		1.25	3.4	
6.	1.28	1.4		1.28	2.7		1.27	3.6	
7.	1.30	1.4		1.30	2.7		1.35	3.8	
8.	1.54	1.0		1.32	2.9		1.70	3.5	
9.	1.58	1.0	Fl.B	1.62	2.6	Fl.B	1.74	3.5	Fl
10.	2.25	1.1		1.64	2.5		2.25	3.5	
11.				1.75	2.5				

	$D_1P_2H_1d_2$			$D_1P_2H_2d_2$			$D_1P_2H_3d_2$		
1.	0.25	0.4		0.3	0.8		0.44	2.0	
2.	0.48	0.7		0.42	1.0		0.62	2.9	
3.	0.60	0.2	FB	0.52	1.3	FB	0.75	3.2	
4.	0.62	1.3		0.72	1.5		0.80	3.6	FB
5.	0.76	1.0		0.75	2.0		0.85	3.7	
6.	1.00	0.9		0.77	2.1		0.90	3.8	
7.	1.42	1.0		1.00	1.6		1.25	3.3	
8.	1.82	1.1		1.20	1.7		1.75	3.3	
9.	2.35	1.3	Fl.B.	1.70	1.9	Fl.B	2.20	3.4	Fl.
10.	-			2.00	2.0		2.50	3.4	
11.	▼								

	$D_1P_3H_1d_2$			$D_1P_3H_2d_2$			$D_1P_3H_3d_2$		
1.	0.25	0.7		0.30	1.7		0.30	1.9	
2.	0.35	1.0	F B	0.35	1.8	F B	0.45	2.9	
3.	0.40	1.1		0.40	2.0		0.50	3.3	
4.	0.42	1.2		0.45	2.1		0.55	3.6	
5.	0.45	1.1		0.50	2.2		0.60	3.7	
6.	0.5	0.7		0.70	2.0		0.80	3.2	
7.	0.75	0.7		0.75	2.0		0.85	3.2	
8.	0.05	0.8	Fl.B	0.05	2.0	Fl.B	1.30	3.2	F
9.	1.25	0.8		1.55	2.1		1.65	3.3	
10.	1.60	0.9		2.00	2.1		2.00	3.4	
11.									

Table No.4.5 Experimental Observations in Cold Model FBR

S.No.	$D_1P_1H_1d_1$ V (cm/sec.)	P_{H_2O} (cm)	Visual Obs.	$D_3P_1H_2d_1$ U (cm/sec)	P_{H_2O} (cm)	Visual	$D_2P_1H_3d_1$ V (cm/sec)	P_{H_2O}	Vi O
1.	0.25	1.2		0.25	2.0		0.27	4.0	
2.	0.37	1.8	F B	0.67	4.0	FB	0.67	7.0	F
3.	0.50	2.4		1.00	5.4		1.22	10.4	
4.	0.63	3.0		1.25	7.0		1.32	11.2	
5.	0.85	3.8		1.26	7.2		1.50	11.8	
6.	0.87	4.0		1.27	7.6		1.52	12.4	
7.	0.91	4.2		1.28	8.0		1.67	12.8	
8.	1.10	3.0		1.77	6.6		1.97	9.6	
9.	1.15	2.8	Fl.B	1.87	6.4	Ch.	2.05	9.8	CH
10.	1.50	2.8		1.97	6.8		2.20	9.8	
11.	2.00	2.8		2.37	7.0		2.29	10.0	
6									

	$D_2P_2H_1d_1$			$D_2P_2H_2h_1$			$D_2P_2H_3d_1$		
1.	0.12	1.0		0.25	2.8		0.27	5.0	
2.	0.50	3.4	FB	0.32	3.0	FB	0.62	9.6	F
3.	0.52	3.8		0.50	4.4		0.67	10.4	
4.	0.60	4.2		0.72	6.0		0.87	11.6	
5.	0.65	4.4		0.82	7.6		0.90	12.0	
6.	0.85	2.8		0.87	8.0		0.95	12.4	
7.	0.87	2.4		0.90	8.6		1.20	10.0	
8.	0.92	2.6		1.25	5.8		1.50	10.0	
9.	1.15	2.4		1.32	5.6		1.77	10.0	
10.	1.50	2.2		1.55	6.0		2.17	10.0	
11.	1.85	2.4	Ch.	2.12	6.2	Ch.	2.62	10.6	

	$D_2P_3H_1d_1$			$D_2P_3H_2d_1$			$D_2P_3H_3d_1$	
1.	0.25	1.4	FB	0.22	3.2	FB	0.22	5.6
2.	0.50	3.0		0.42	6.0		0.50	9.4
3.	0.55	3.4		0.62	7.8		0.62	11.0
4.	0.62	3.8		0.67	8.2		0.77	12.4
5.	0.67	4.6		0.87	6.0		0.82	13.0
6.	0.80	4.6		0.97	5.8		0.87	13.2
7.	0.95	2.8		1.25	6.0		1.25	10.6
8.	1.00	2.8	Ch.	1.42	6.2	Ch	1.25	10.2
9.	1.10	2.6		1.80	6.4		1.37	10.2
10.	1.27	3.0		2.25	6.6		1.75	10.2
11.	1.37	3.0		2.55	7.0		2.17	10.4

Table No. 4.6 Experimental Observations in Cold Model FBR

S.No.	$D_2P_1H_1d_2$ U (cm/Sec)	H_2O (cm)	Visual obs.	$D_2P_1H_2d_2$ V (cm/sec)	P H_2O (cm)	Visual	$D_2P_1H_3d_2$ V Obs (cm/Sec)	P H_2O cm	Vi O
1.	0.62	0.8		0.62	1.4		0.50	1.9	
2.	0.87	1.0	F B	0.87	1.9	FB	0.82	2.5	FB
3.	1.00	1.2		1.05	2.2		1.05	3.0	
4.	1.10	1.3		1.17	2.4		1.17	3.3	
5.	1.17	1.4		1.22	2.5		1.25	3.6	
6.	1.22	1.3		1.27	2.6		1.32	3.7	
7.	1.25	1.5		1.32	2.8		1.37	3.8	
8.	1.50	1.2		1.55	2.1		1.62	3.1	
9.	1.60	1.2		1.60	2.1		1.67	3.0	
10.	1.72	1.3	F1.B	2.00	2.2	Ch	1.92	3.2	Ch
11.	1.90	1.3		2.35	2.3		2.32	3.3	

	$D_2P_2H_1d_2$			$D_2P_2H_2d_2$			$D_2P_2H_3d_2$		
1.	0.25	0.5		0.25	1.0	FB	0.30	1.8	FI
2.	0.37	0.9		0.42	1.4		0.50	2.5	
3.	0.45	1.0	FB	0.57	1.7		0.62	2.9	
4.	0.50	1.2		0.62	1.9		0.77	3.3	
5.	0.60	1.4		0.67	2.2		0.85	3.6	
6.	0.62	1.5		0.75	2.3		0.90	3.9	
7.	0.67	1.5		0.77	2.4		0.95	3.9	
8.	0.82	1.8	F1B	0.05	1.7	Ch	1.12	3.2	Ch.
9.	0.95	1.2		1.05	1.7		1.20	3.1	
10.	1.35	1.2		1.40	1.7		1.87	3.1	
11.	1.72	1.3		2.02	1.9		2.25	3.3	

	$D_2P_3H_1d_2$			$D_2P_3H_2d_2$			$D_2P_3H_3d_2$		
1.	0.17	0.7		0.17	1.1	FB	0.25	2.3	FB
2.	0.25	0.9	FB	0.25	1.4		0.42	3.0	
3.	0.35	1.0		0.37	2.0		0.55	3.5	
4.	0.37	1.2		0.45	2.3		0.51	3.7	
5.	0.40	1.3		0.50	2.4		0.62	3.8	
6.	0.45	1.4		0.55	2.5		0.67	3.9	
7.	0.57	1.1		0.70	2.0		0.87	3.0	
8.	0.62	1.0	F1.B	0.72	1.9	Ch	0.87	3.0	C
9.	0.85	1.0		0.77	1.8		0.92	3.0	
10	1.05	1.0		0.92	1.9		1.25	3.2	
11.	1.59	1.0		1.27	2.1		2.12	3.3	

TableNo.4.7 Experimental Observations in Cold Model F B R

	$D_3P_1H_1d_1$			$D_3P_1H_2d_1$			$D_3P_1H_3d_1$		
S.No.	V (cm/sec)	P H_2Ocm	Visual Obs.	V (cm/sec)	P H_2O(cm)	Visual Obs.	V (cm/sec)	P H_2O (cm)	Visual Obs.
1.	0.37	1.2		0.75	3.0		0.68	5.0	
2.	0.46	1.5	FB	1.14	6.1	FB	1.10	7.4	FB
3.	0.57	1.8		1.50	7.4		1.45	9.6	
4.	0.77	2.4		1.60	7.8		1.85	11.4	
5.	1.05	3.2		1.70	8.0		2.05	12.1	
6.	1.12	3.7		1.80	8.5		2.10	12.4	
7.	1.20	4.0	Fl.B	2.15	6.3	Fl.B	2.20	12.6	Fl.B.
8.	1.28	4.3		2.25	6.5		2.45	10.4	
9.	1.55	2.6		2.40	6.2		2.52	10.4	
10.	1.69	2.5		2.65	6.4		2.78	10.3	
11.	2.05	2.2		2.87	6.6		3.18	10.4	
	$D_3P_2H_1d_1$			$D_3P_2H_2d_1$			$D_3P_2H_3d_1$		
1.	0.16	1.2	FB	0.27	5.8	FB	0.25	6.0	
2.	0.22	2.6		0.48	7.2		0.50	9.0	FB
3.	0.48	3.8		0.50	7.6		0.65	11.0	
4.	0.50	4.5		0.58	8.3		0.70	11.4	
5.	0.58	4.5		0.65	9.0		0.75	11.6	
6.	0.72	2.8	Fl.B	0.85	6.0	Ch.	0.80	12.0	
7.	0.73	2.3		0.90	6.0		0.82	12.4	Ch
8.	1.05	2.2		1.05	6.0		0.97	9.2	
9.	1.40	2.5		1.30	6.1		1.12	9.2	
10.	1.72	2.2		1.55	6.0		1.50	9.2	
11.	2.00	2.2		2.00	6.2		2.00	9.3	
	$D_3P_3H_1d_1$			$D_3P_3H_2d_1$			$D_3P_3H_3d_1$		
1.	0.15	1.0		1.0	0.15		0.16	6.0	
2.	0.25	2.0	FB	2.0	0.25	FB	0.25	7.4	FB
3.	0.35	3.0		3.0	0.35		0.35	8.8	
4.	0.40	3.4		3.4	0.40		0.40	10.0	
5.	0.45	3.8		3.8	0.50		0.45	11.0	
6.	0.55	2.6		3.8	0.55		0.50	12.0	
7.	0.60	2.4		2.8	0.65	Ch	0.60	12.4	Ch
8.	0.85	2.4	Fl.B	2.6	0.70		0.65	13.4	
9.	115	2.4		2.4	0.85		1.00	9.0	
10.	1.55	2.4		2.4	0.89		1.30	9.0	
11.	2.00	2.5		2.5	1.00		1.75	9.4	

Table No. 4.8 Experimental Observations in Cold Model F B R.

		$D_3P_1H_1d_2$		$D_3P_1H_2d_2$		$D_3P_1H_3d_2$		
S.No.	V (Cm/sec)	P H_2Ocm	Visual Obs.	V (cm/sec.)	P H_2O(cm)	Visual obs.	V (cm/sec)	P H_2Ocm	Visual obs.
1.	0.45	0.6		0.65	1.6		0.50	1.4	
2.	0.65	0.8	FB	0.90	2.0	F B	0.70	2.0	FB
3.	0.90	1.2		1.10	2.3		0.90	2.6	
4.	1.05	1.3		1.17	2.6		1.12	3.0	
5.	1.12	1.4		1.25	2.6		1.20	3.2	
6.	1.20	1.4		1.30	2.7		1.30	3.4	
7.	1.25	1.6	Fl.B	1.32	2.7	Fl.B	1.35	3.6	Ch
8.	1.50	1.3		1.35	2.7		1.40	3.7	
9.	1.55	1.2		1.60	2.4		1.50	3.8	
10.	1.65	1.3		1.70	2.4		1.65	3.3	
11.	2.20	1.4		1.70	2.3		1.67	3.2	

		$D_3P_2H_1d_2$		$D_3P_2H_2d_2$		$D_3P_2H_3d_2$		
1.	0.30	0.6		0.25	0.8		0.25	1.4	
2.	0.45	0.8		0.47	1.4		0.40	2.0	F B
3.	0.55	1.1	FB	0.60	1.8	FB	0.50	2.4	
4.	0.57	1.2		0.70	1.9		0.65	3.0	
5.	0.62	1.3		0.72	2.0		0.70	3.2	
6.	0.70	1.3		0.75	2.2		0.72	3.3	
7.	0.80	1.1		0.90	1.7		0.75	3.3	
8.	0.90	1.0	Fl B	0.95	1.6		0.80	3.4	Fl.B
9.	1.30	1.1		1.10	1.7	Fl.B	0.82	3.6	
10.	1.40	1.2		1.50	1.7		0.85	3.9	
11.	1.80	1.2		1.85	2.0		0.90	3.9	

		$D_3P_3H_1d_2$		$D_3P_3H_2d_2$		$D_3P_3H_3d_2$		
1.	0.20	0.6	F B	0.20	1.2		0.20	1.6	
2.	0.25	0.8		0.35	1.8	FB	0.35	2.4	FB
3.	0.30	1.1		0.40	2.0		0.50	3.2	
4.	0.35	1.2		0.45	2.2		0.55	3.3	
5.	0.40	1.3		0.50	2.4		0.60	3.4	
6.	0.45	1.0		0.55	2.5		0.65	3.6	
7.	0.55	0.9		0.70	1.9	Ch.	0.70	3.7	
8.	0.60	1.0	Fl.B	0.72	1.8		0.90	3.2	Ch.
9.	1.00	1.0		1.15	2.0		0.95	3.1	
10.	1.25	1.0					1.45	3.2	
11.							1.80	3.3	

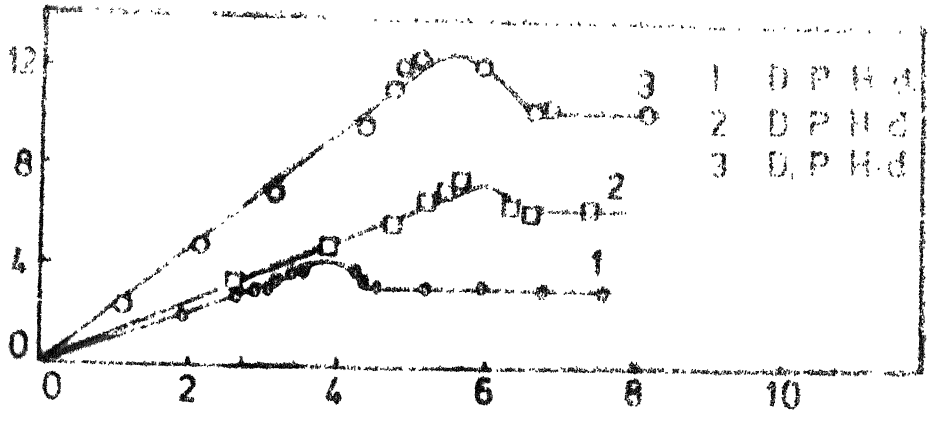

Fig. 4.5. ΔP- velocity plot

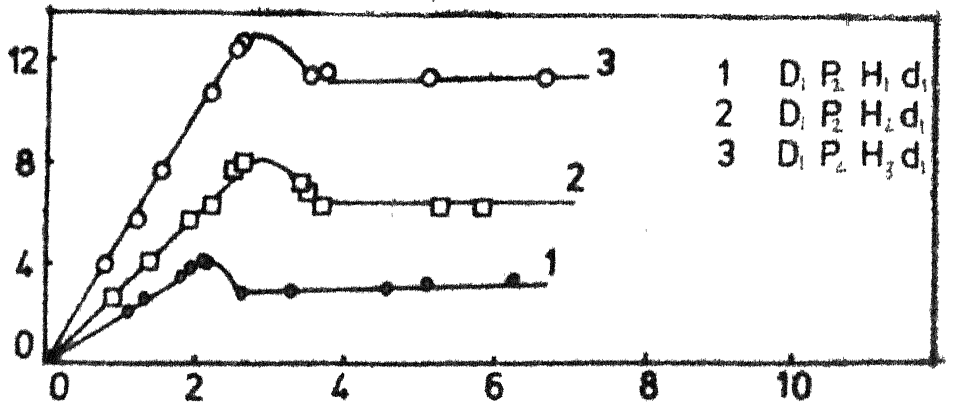

Fig. 4.6. ΔP- velocity plot

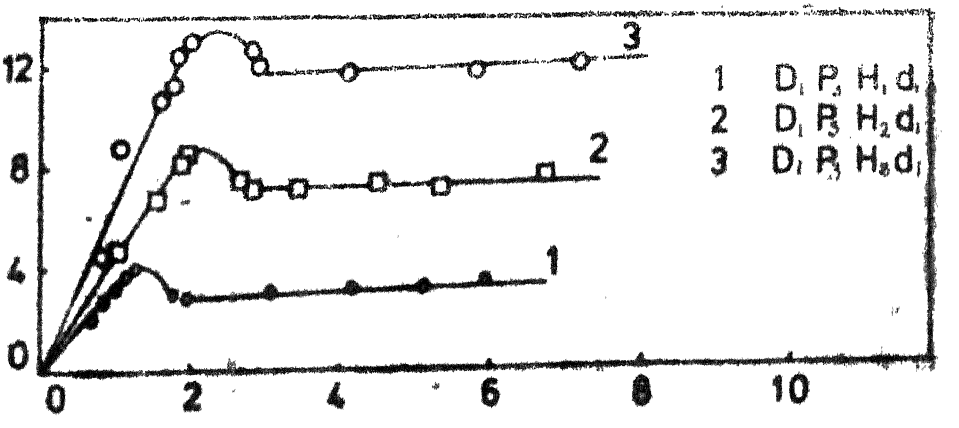

Fig. 4.7. ΔP- velocity plot

Pressure drop (cms of H_2O)

Velocity (cms / sec)

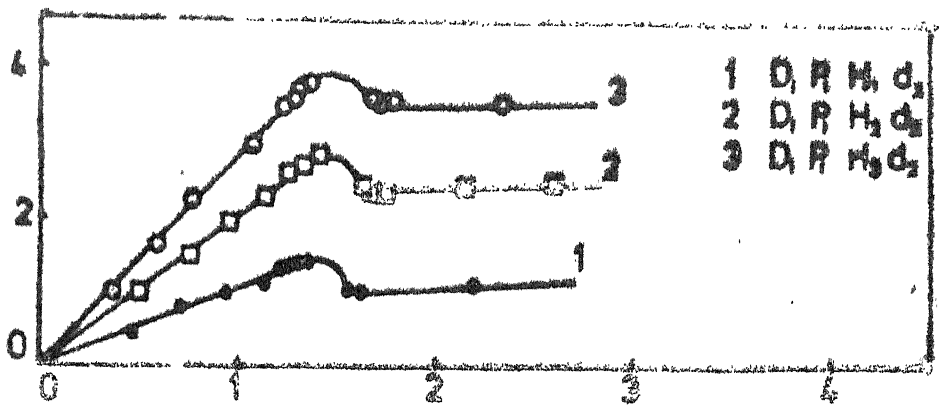

Fig.4.8. ΔP- velocity plot

Pressure drop (cms of H_2O)

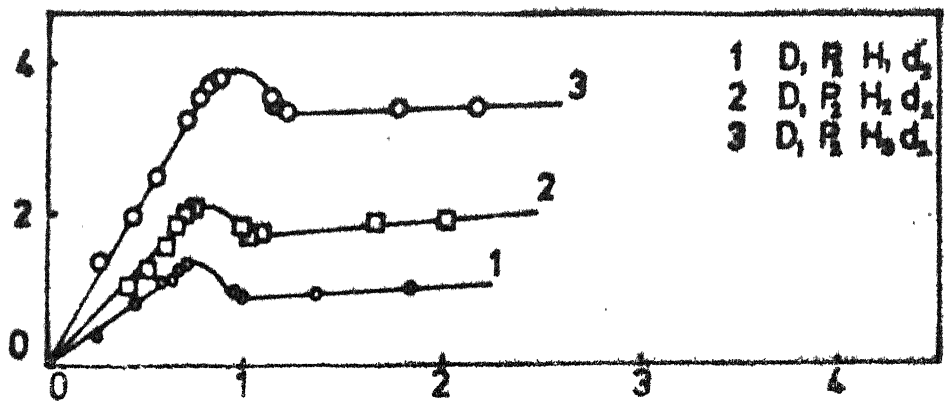

Fig.4.9. ΔP- velocity plot

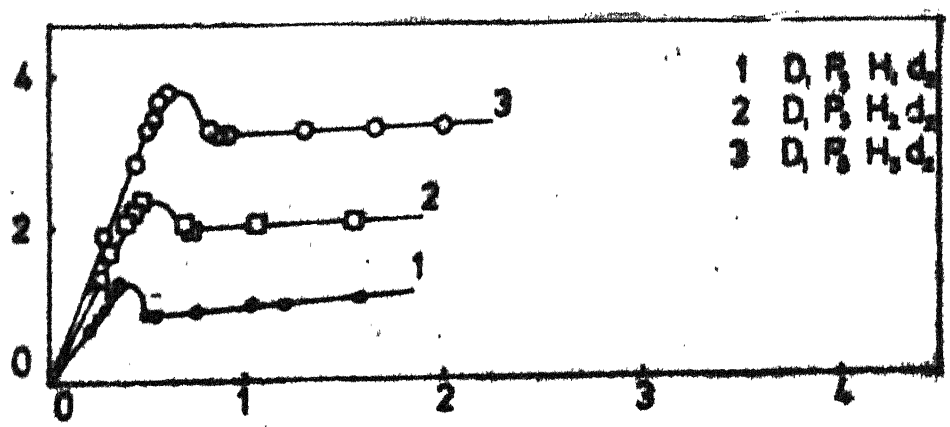

Fig.4.10. ΔP- velocity plot

Velocity (cms / sec)

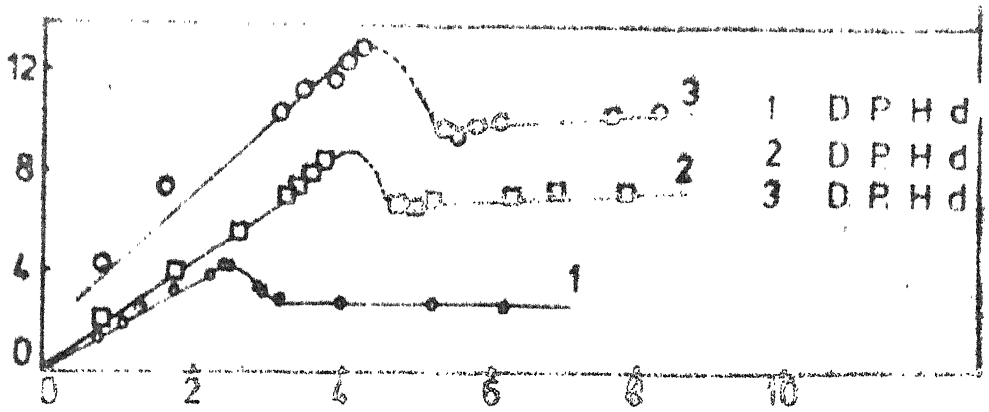

Fig. 4.11. ΔP- velocity plot

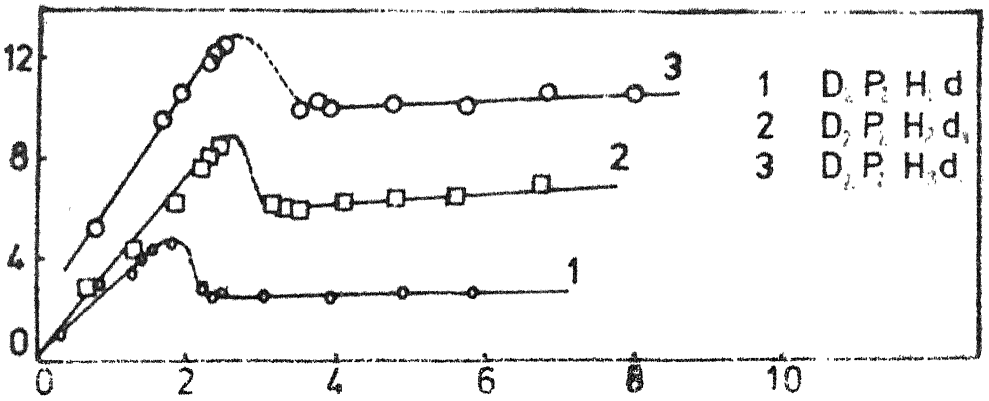

Fig. 4.12. ΔP- velocity plot

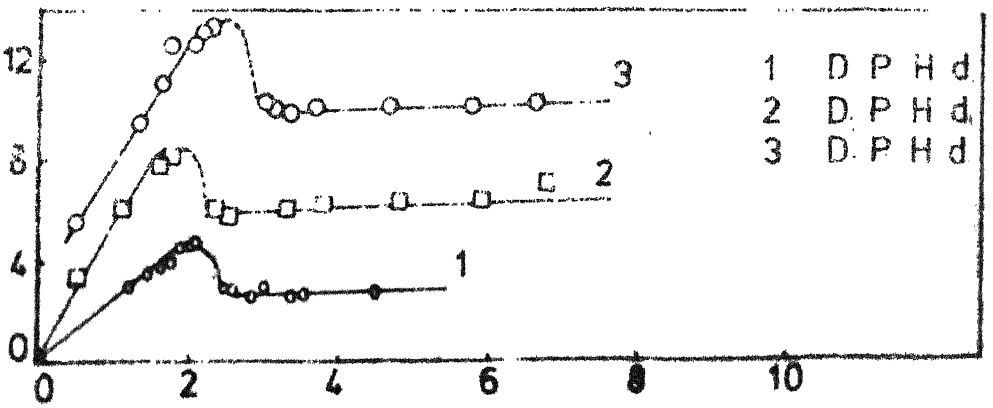

Fig 4.13 ΔP- velocity plot

Pressure drop (cms of H_2O)

Velocity (cms / sec)

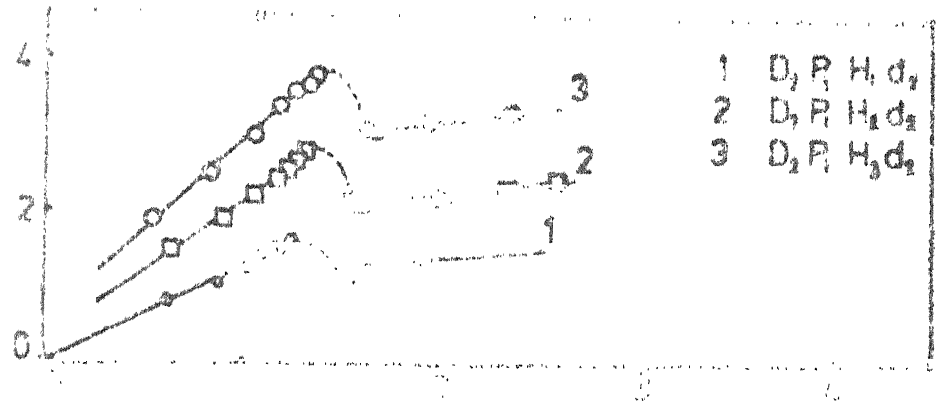

Fig. 4.14 ΔP- velocity plot

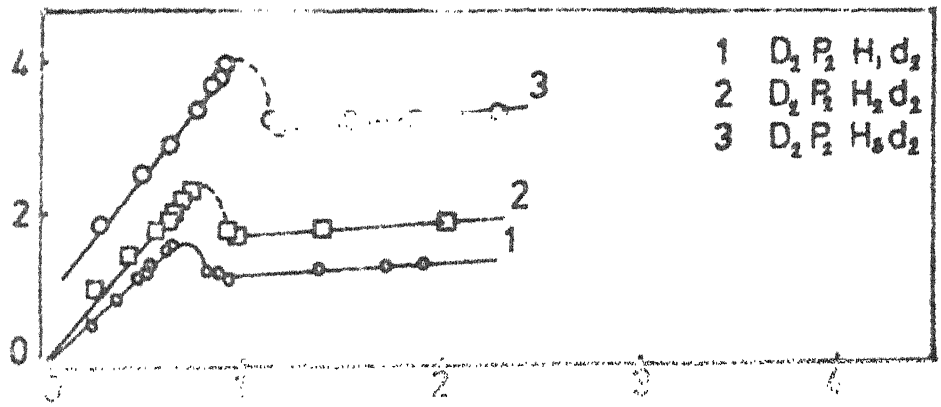

Fig. 4.15. ΔP- velocity plot

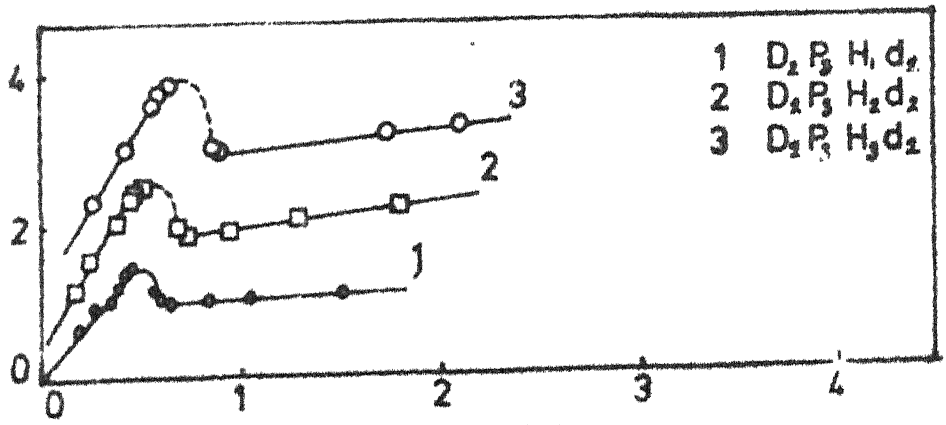

Fig. 4.16. ΔP - velocity plot

Pressure drop (cms of H_2O)

Velocity (cms / sec)

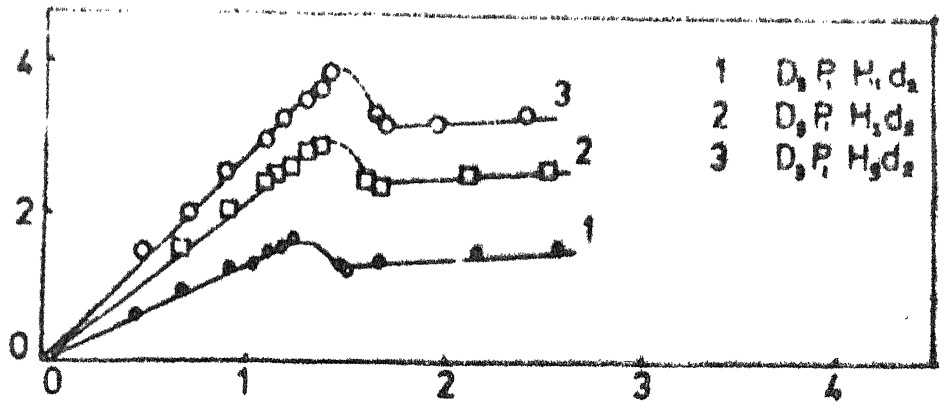

Fig.4.17. ΔP- velocity plot

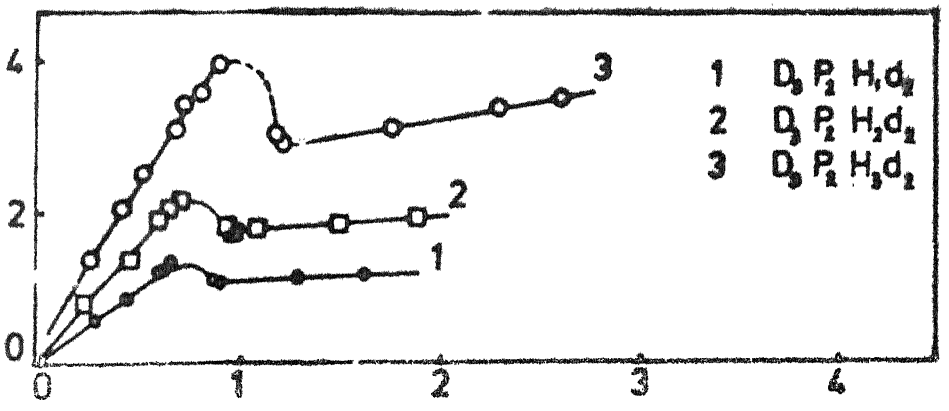

Fig.4.18 ΔP- velocity plot

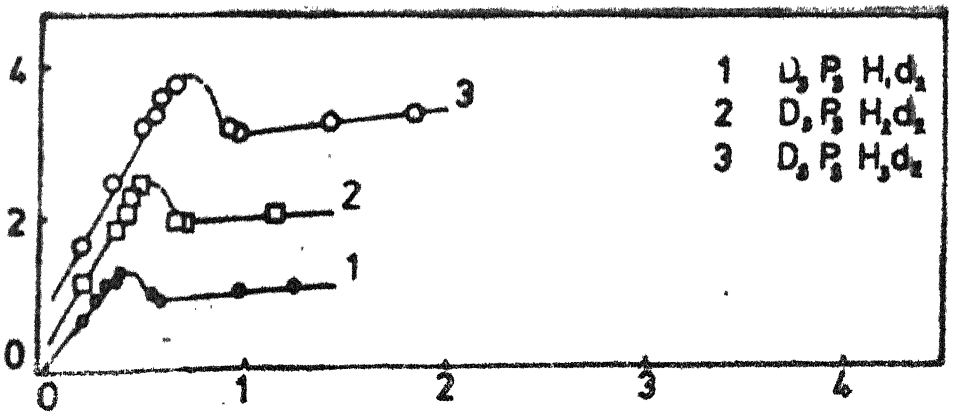

Fig.4.19. ΔP- velocity plot

Pressure drop (cms of H_2O)

Velocity (cms / sec)

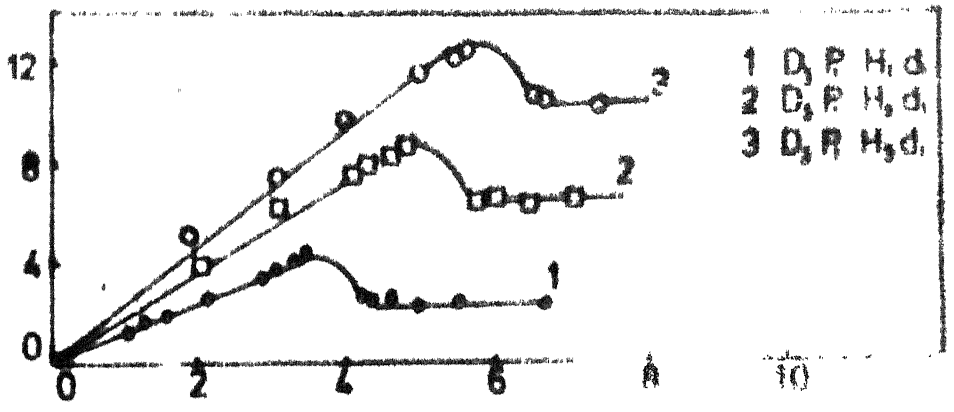

Fig.4.20. ΔP- velocity plot

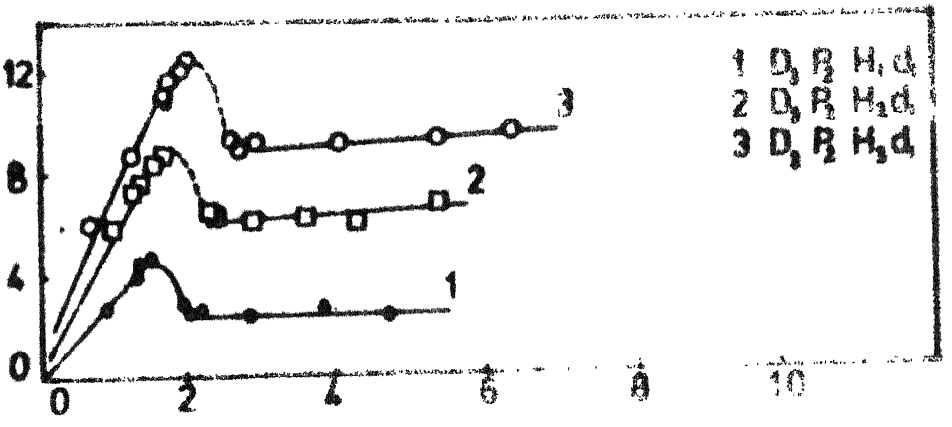

Fig.4.21. ΔP- velocity plot

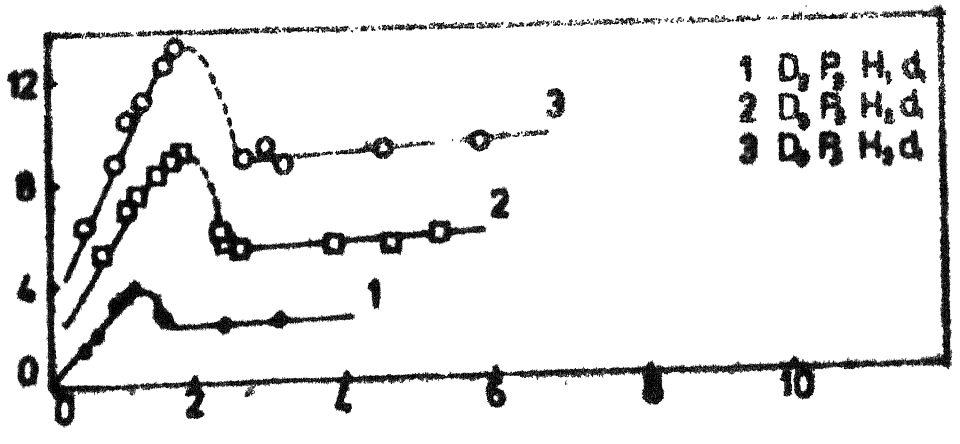

Fig.4.22. ΔP- velocity plot

Pressure drop (cms of H_2O)

Velocity (cms / sec)

Occurrence of channelling with D_2 and D_3 distributors is attributed to the improper distribution of perforations in these distributor plates. It was also noted that the channelling usually occurred near the wall of reactor.

These observations lead to the conclusion that the distributors D_2 and D_3 were poorly designed and that the performance of the distributor D_1 was the best amongst the three distributors considered.

EFFECT OF PARTICLE SIZE

The effect of particle size on fluidization behaviour is considered in terms of u_{mf} which can be predicted using Eqs. (2.7) & (2.8) for different ranges of flow rates. For low flow rates of gas ($Re_p < 20$) u_{mf} is proportional to the square of particle size, where as for high gas flow rates u_{mf} is proportional to the particle size.

The variation of pressure drop with particle size can be predicted using Eqs. (2.2) and (2.3). For $Re_p < 20$, pressure drop is inversely proportional to the squares of particle size but inversely proportional to particle size for $Re_p > 1000$. All the experiments which have been carried out are in range $Re_p < 20$ and hence we shall confine ourselves to Eqs. (2.12) and (2.13) for the prediction of u_{mf} and Eq. (2.2) for the prediction of ΔP. The experimentally determined and theoretically estimated values of u_{mf} and ΔP for hematite and sand, respectively are tabulated in Tables 4.9-4.10. It is seen that the

Table No.4.9 Comparison of Theoritical &Experimental values of U_{mf}, ΔP for Hematite

Sl. No.	Distributor Particle size in mesh	Bed Height in cms.	Combination	U_{mf} (Cm/sec.) Theo.	U_{mf} (Cm/sec.) Exp.	ΔP (cms. of H_2O) Theo.	ΔP (cms. of H_2O) Exp.
1.	P_1-72+100	2	$D_1P_1H_1d_1$		4.0	4.19	4.0
		4	$D_1P_1H_2d_1$	4.53	5.2	8.59	7.2
D_1		6	$D_1P_1H_3d_1$		5.3	13.20	12.4
	P_2-100+150	2	$D_1P_2H_1d_2$		2.3	4.39	4.0
		4	$D_1P_2H_2d_1$	2.22	2.6	9.00	8.0
		6	$D_1P_2H_3d_1$		2.6	13.82	12.8
	P_3-150+170	2	$D_1P_3H_1d_1$	1.31	1.4	4.61	4.0
		4	$D_2P_1H_2d_1$	[illegible]	2.1	9.43	8.6
		6	$D_1P_3H_3d_1$		2.2	14.77	13.1
2.	P_1-72+100	2	$D_2P_1H_1d_1$		2.7	4.19	4.0
		4	$D_2P_1H_2d_1$	4.53	4.0	8.59	8.6
D_2		6	$D_2P_1H_3d_1$		4.2	13.20	12.8
	P_2-100+150	2	$D_2P_2H_1d_1$		2.1	4.39	4.2
		4	$D_2P_2H_2d_1$	2.22	2.6	9.00	8.8
		6	$D_2P_2H_3d_1$		2.7	13.82	12.8
	P_3-150+170	2	$D_2P_3H_1d_1$		2.2	4.61	4.4
		4	$D_2P_3H_2d_1$	1.31	2.0	9.43	8.2
		6	$D_2P_3H_3d_1$		2.15	14.77	13.4
3.	P_1-72+100	2	$D_3P_1H_1d_1$		3.8	4.19	4.1
		4	$D_3P_1H_2d_1$	4.53	4.7	8.59	8.6
D_3		6	$D_3P_1H_3d_1$		5.1	13.82	12.9
	P_2-100+150	2	$D_3P_1H_1d_1$		1.7	4.59	4.1
		4	$D_3P_2H_2d_1$	2.22	1.9	9.00	9.0
		6	$D_3P_2H_3d_1$		2.0	13.82	12.9
	P_3-150+170	2	$D_3P_3H_1d_1$		1.3	4.61	4.0
		4	$D_3P_3H_2d_1$	1.31	1.7	9.43	8.8
		6	$D_3P_3H_3d_1$		1.7	14.77	13.4

S.No.	Distributor plate	Particle size in mesh	Bed Height (cm)	Combination	U_{mf} (cm/sec)	ΔP for Sand, U_{mf} (cm/sec) Theo-	Exp.	ΔP (cm. of H_2O) Theo.	Exp.
1.	D_1	P_1:-72+100	2	$D_1P_1H_1d_2$	1.306	1.40	1.20		1.3
			4	$D_1P_1H_2d_2$	1.306	1.45	2.52		2.8
			6	$D_1P_1H_3d_2$		1.50	3.87		3.9
		P_2:-100+150	2	$D_1P_2H_1d_2$		0.70	1.26		1.3
			4	$D_1P_2H_2d_2$	0.641	0.75	2.58		2.2
			6	$D_1P_2H_3d_2$		0.80	3.96		3.9
		P_3:-150+170	2	$D_1P_3H_1d_2$		0.35	1.29		1.3
			4	$D_1P_3H_2d_2$	0.378	0.50	2.70		2.4
			6.	$D_1P_3H_3d_2$		0.65	4.14		3.8
2.	D_2	P_1:-72+ 100	2	$D_2P_1H_1d_2$		1.30	1.20		1.6
			4	$D_2P_1H_2d_2$	0.306	1.35	2.52		2.7
			6	$D_2P_1H_3d_2$		1.35	3.87		3.9
		P_2:-100+150	2	$D_2P_2H_1d_2$		0.75	1.26		1.3
			4	$D_2P_2H_2d_2$	0.641	0.80	2.58		2.4
			6	$D_2P_2H_3d_2$		0.90	3.96		4.0
		P_3:-150+170	2	$D_2P_3H_1d_2$		0.45	1.29		1.4
			4	$D_2P_3H_3d_2$	0.378	0.50	2.70		2.6
			6	$D_2P_3H_3d_2$		0.65	4.14		4.0
3.	D_3	P_1:-72+100	2	$D_3P_1H_1d_2$		1.30	1.20		1.6
			4	$D_3P_1H_2d_2$	1.306	1.40	2.52		2.9
			6	$D_3P_1H_3d_2$		1.45	3.87		4.0
		P_2:-10.+150	2	$D_3P_2H_1d_2$		0.75	1.26		1.3
			4	$D_3P_2H_2d_2$	0.641	0.75	2.58		2.2
			6	$D_3P_2H_3d_2$		0.90	3.96		3.9
		P_3:-150+170	2	$D_3P_3H_1d_2$		0.35	1.29		1.2
			4	$D_3P_3H_2d_2$	0.378	0.45	2.70		2.5

experimental values of u_{mf} and ΔP are in reasonable agreement with those predicted for both sand and hematite though the agreement is better in the use of sand. Somewhat superior agreement in the case of sand is perhaps due to the free flowing nature of sand, and the fact that the sand particles are, in general spherical.

EFFECT OF MATERIAL

It is obvious from Eqs. (2.12) and (2.13) that both u_{mf} and ΔP are proportional to the difference in the densities of solid and gas for the entire range of Reynolds number. Therefore, the sand which is lighter than hematite will have comparatively lower u_{mf} and ΔP values. The experimental and theoretical values of these two parameters for the two materials are tabulated in Tables 4.9-4.10.

Once again reasonably good agreement between the theoretical and predicted values is observed. For the irregular and non-free flowing hematite particles the discrepancy between the experimental and theoretical values is somewhat higher. It is further observed that the flowability of hematite increases with particle size. This could be one of the reasons for pronounced channelling that was observed in the case of particles finer than 100 mesh.

EFFECT OF BED HEIGHT (1,3,14)

The effect of bed height on the pressure drop of the bed can be predicted using Eqs. (2.2),(2.3) and (2.6).

The pressure drop across the bed is proportional to the bed height whereas the theoretical u_{mf} is independent of the bed height. Experimental values in the present investigation (Tables 4.9-4.10) however, record a slight deviation in u_{mf} values with increasing bed height, though it increases only slightly. This discrepancy is attributed to the frictional effects which increases with increasing height and which have been ignored in the theoretical equations.

On the basis of experimental investigation of the cold model FBR, presented in this chapter, it could be concluded that the design of the distributor D_1 was the best. This design was therefore chosen for the high temperature FBR described in the following chapter.

CHAPTER - 5

DESIGN AND FABRICATION OF HIGH TEMPERATURE FBR

Based on the results of the cold model FBR studies, the high temperature FBR was designed and fabricated. Greater emphasis was laid on the choice of the distributor plate which plays a critical role in all fluidized beds.

A close matching of the design dimensions of the high temperature FBR with that of the cold model was aimed at. Any deviation from the cold model was likely to alter the fluidization characteristics. Nonetheless, it was found necessary to make some alterations in the design. A major alteration was effected in the preheater design. This modification is discussed in the following paragraph.

5.1 PREHEATER DESIGN

The gas-solid reactions may be endothermic or exothermic. In general, the reduction reactions are endothermic. Hence it may be necessary to preheat the gases to the reaction temperature. As the proposed FBR was to be used for the reduction of hematite using either coke and some inert gas, or hydrogen, it was essential to preheat the gas to the reaction temperature. In order to heat the gas from room temperature to a temperature as high as 800-900°C, the length of the preheater is important. Preheating of gas to the desired temperature is a function of its residence time in the preheater which, in turn, depends on the length

of the preheater and the gas velocity. Since the fluidized beds are generally operated at 5-20 times the minimum fluidization velocity[1,2], sufficiently long preheater would be required.

The preheater designed for our work was made of 70 cms long and 5.2 cms diameter stainless steel tube, which could be independently heated up by enclosing it in a Kanthal wire wound tube furnace. Because of the non-availability of a long enough furnace which could contain both the preheater and the reactor, it became necessary to separate the preheater from the main reactor. The preheater tube was completely filled up with ½" mild steel balls to enhance the heat transfer from the preheater to the flowing gas, because of the high heat content of these balls. It also resulted in increased residence time because of torturous path that the gas would now have to take.

Both the bottom and top ends of the preheater tube were connected to stainless steel heads. Through the top head the preheater was connected to the main reactor where as the bottom head was used to provide the fluidizing gas to be preheated.

5.2 REACTOR DESIGN

The dimensions of the main reactor were exactly the same as that of the cold model FBR. The reactor was 60 cms long and 5.2 cms diameter. It was made of [illegible] stainless steel tube. The distributor plate

was fitted at the bottom of the reactor using screws and nuts.

A stainless steel head covered the top part of the reactor tube which was outside the furnace. This stainless steel head could be tightened on to the tube with the help of flanges and screws. Three openings were provided in this head. A stainless steel tube welded to the head through the opening and the center of tube provided on outlet for the gases. Through one of the other openings a Chromel-Alumel thermocouple could be introduced into the reactor in such a way that its tip was just 1 cm above the distributor plate. This arrangement was to ensure that the tip of the thermocouple remained dipped in the fluidized bed and the exact reaction temperature could be recorded during the reduction experiments.

The third opening on the head was for introducing the solid powder sample to the reactor. This hole could be sealed with a high temperature silicon rubber cork immediately after the sample was introduced.

The outlet stainless steel tube was brazed with 1.5 m long, 1.25 cm diameter copper tube with an objective to cool the exit gases to the room temperature.

The bottom of the main reactor was connected to a 5.2 cm diameter and 10 cm long stainless steel tube with t help of flanges and screws. This tube was filled up with ½" mild steel balls to ensure uniform distribution of

The reactor assembly was connected with the help of 1 cm diameter, 25 cm long stainless tube to the preheater assembly. This tube was heavily insulated with the help of asbestos cloth and Alumina bricks so as to minimize heat losses.

All the joints in the reactor and preheater assembly were provided with gaskets made of high temperature materials and these were sealed with high temperature sealant to make the reactor leak proof.

The schematic diagram of complete FBR assembly with preheater is shown in Fig. 5.1.

5.3 EXPERIMENTAL SET UP

Two furnaces were designed, one each for FBR and Preheater. The furnace tubes were made of Alumina, were 7.6 cms in diameter and 60 cms in length.

The preheater furnace was Kanthal wire wound furnace, of total resistance of 40 ohms, with a power output of 1.25Kwatts. This was designed to produce a temperature of 800-900°C.

Six silicon carbide rods, each of one ohm resistance, were used as heating element in the reactor furnace. The power output of this furnace was almost twice that of the preheater furnace. A temperature as high as 1200°C could be achieved in this furnace.

Both the furnaces were arranged one above the other (preheater occupying the top position) such that

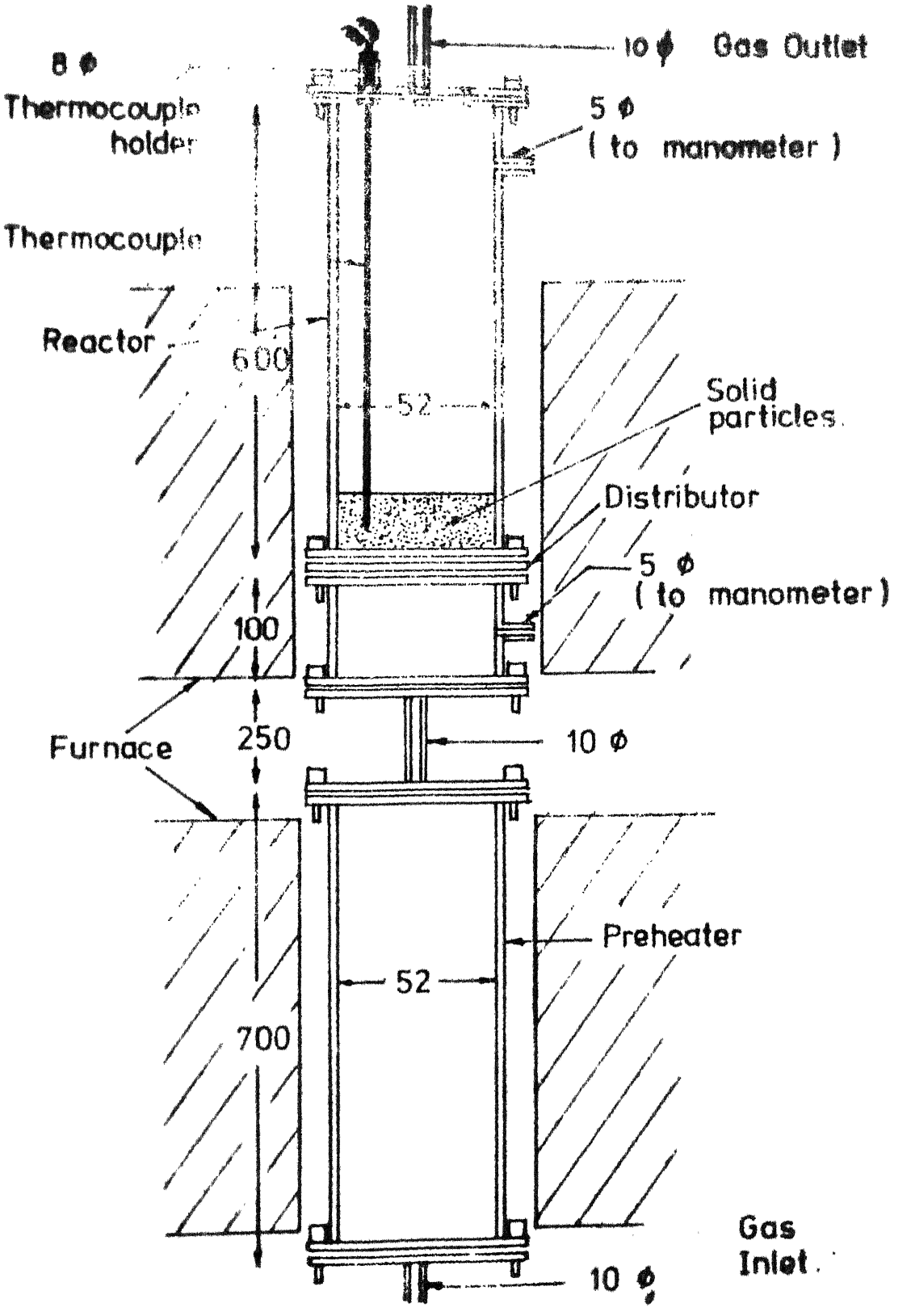

Fig 5.1 High Temperature FBR details

their axes alligned. The furnaces were separated by a distance of 25 cms.

The FBR-preheater assembly was introduced into the furnace such that the reaction zone in the reactor exactly coincided with the constant temperature zone of the furnace.

A copper gauze furnace was used to remove oxygen impurities from the fluidizing gas before it enters the preheater. A rotameter was provided to measure the flow rate of the inlet gas.

The outlet from the reactor was connected to a water trap with the help of a rubber tube. Any entrained solid particles could be removed here. The gas from water trap was connected to a series of gas samplers through a capiliary flowmeter. This capiliary flowmeter was used to measure the flow rate of outlet gases.

Due to some problems with our chromatograph, it could not be possible to analyze the gas sample immediately during the experiment. So an assembly of gas samplers, which was connected to the capiliary flowmeter, had to be used to store the gas samples collected at different time intervals of the experiment. These samples could be analyzed later using the gas chromatograph.

The schematic diagram of the experimental set up is as shown in Fig. 5.2.

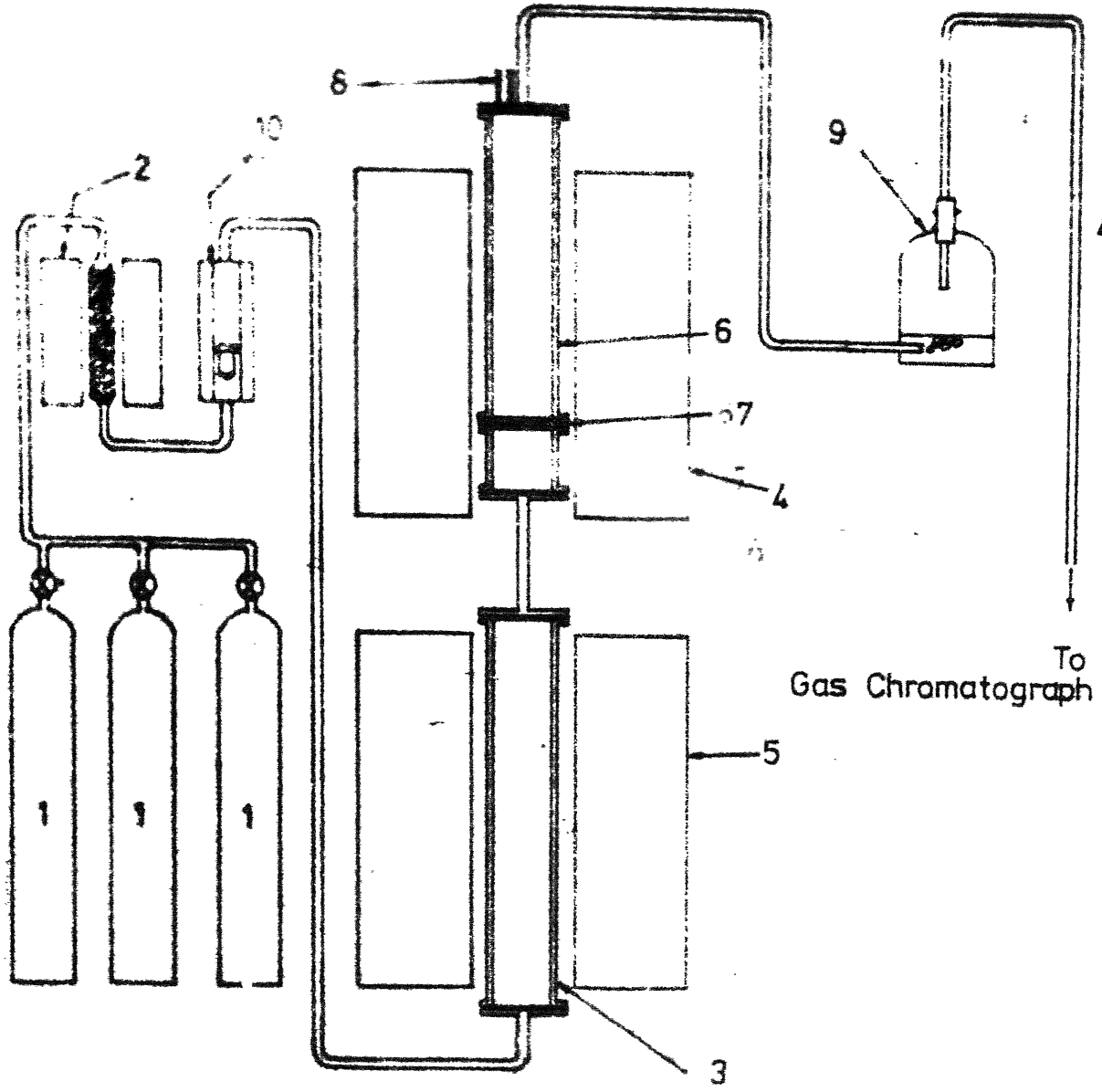

Details of set-up

1. Gas Cylinders
2. Copper Gauze Furnace
3. Pre heater
4, 5 Furnaces
6. Fluidized Bed Reactor
7. Distributor Plate
8. Thermocouple Holder
9. Water Trap
10. Rotameter

High Temperature Model Fluidised Bed Reactor Set-up

Unlike the cold model FBR, in the final design of the high temperature FBR, there was no provision for measuring the pressure drop across the distributor plate and the bed of solid particles, though the same was provided in the initial design of the reactor.

The outlets required for ΔP measurements had to be removed (permanently welded) due to various practical problems. However, before doing that, ΔP vs gas velocity data was generated using the original high temperature FBR at room temperature to ensure that atleast at room temperature its fluidizing behaviour was similar to that of cold model FBR.

CHAPTER - 6

As it was mentioned earlier, the main aim of this investigation was to study the reduction of hematite in FBR. Originally, it was intended to study the reduction of hematite with

(i) Coke using some inert gas as fluidizing medium.

(ii) Coke using methane and nitrogen mixture as fluidizing medium.

However, due to some unsermountable problems with the chromatograph the online analysis of the flue gases containing $CO-CO_2$ could not be possible. Therefore, only a limited number of experiments could be carried out. Reduction of hematite with coke using inert gas as the fluidizing medium could be examined only qualitatively in a few experiments. The problem of reduction with coke and methane was completely dropped. Instead, the reduction with hydrogen was carried out. But since the set up for methane generation and storage was already designed, fabricated and even tested before this change in problem was made it is described below.

METHANE GENERATION AND STORAGE (16)

Fig. (5.1) shows the set up for generation and storage of methane.

A mixture of sodium acetate and 80gms of soda lime was properly ground and mixed and was poured in a pyrex tube (2). The pyrex tube (2) was then gradually insented in the furnace (1) which had already attained the required temperature (i.e. 400°C). When the gas generation rate became appreciable, stop cock (6) was opened and the valve V_3 was detached from the pressurizing water tank (9). The outlet of the water tank (9) which got isolated from V_3 was clamped so that water does not flow out of the tank. The valve V_2 was also kept closed but the valve V_1 was kept open to record the pressure of methane. When the rate of methane generation became too high or too low as could be understood from both the water trap (8) and safety valve (5), the valve V_3 was manipulated to decrease or increase the exit water flow rate accordingly so that the methane generation and storage could take place at slightly above atmospheric pressure. After the completion of the methane generation, the stop cock (6) was closed and the valve V_3 was again connected to the water tank (9) to the storage vessel (7) and compressed the methane gas. The compressed gas thus became ready for use. The flow of methane was maintained almost constant because of inflow of water from the overhead tank (9) into the storage vessel (7). The water level in the overhead tank (9) was maintained constant by ensuring overflow all the time.

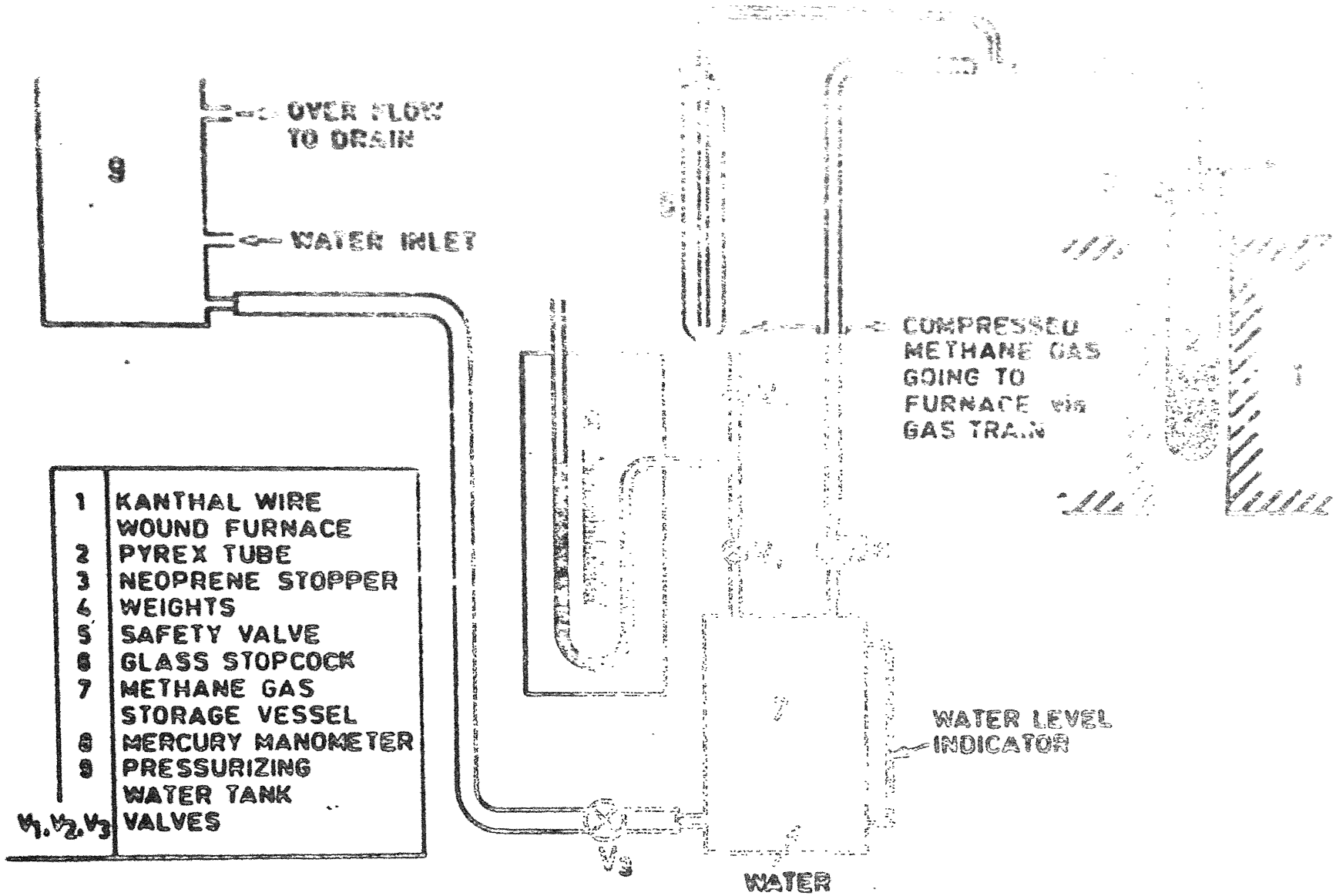

FIG 6.1 SET-UP FOR GENERATION AND STORAGE OF METHANE GAS.

With 100 gms of sodium acetate and 80 gms of soda lime, methane generation was approximately 30 lts at STP. Pressurised methane attained approximately a pressure of [illegible] atmosphere.

[illegible]

In all four experiments with coke as a reducing agent and nine experiments with hydrogen as a reducing agent could be carried out. The experimental conditions employed in these experiments are described in Table 6.1 and 6.2.

The following is the sequence of the operation carried out during the reduction studies in FBR.

The preheater and reactor furnaces were switched on and set to required voltage. Sufficient time was allowed for the attainment and stabilization of the set temperature. The furnace temperature was more precisely controlled using a Chromel-Alumel temperature controller where as the preheater furnace was controlled by adjusting the power input to the furnace.

After flushing the reactor with an inert gas a dried and weighed sample was introduced into the reactor from top with the help of a funnel.

In the first set of experiments involving coke as the reducing agent the sample was a mixture of 100 gm of hematite and 25 gms of coke where as in the second set of experiments involving hydrogen as a reducing agent it consisted of 100 gm of hematite only.

After introduction of the sample into the reactor it was first flushed with the inert gas for a few minutes at low flow rate (below the minimum fluidization velocity). When the reactor temperature was stabilised, the flow of fluidising gas was started at a predetermined rate.

In the case of hydrogen as reducing agent, the effluent gases were collected at regular interval of time in specially designed gas sampler. Variation of reaction temperature during the experiment was also regularly recorded. The fluctuation in temperature was around ±5°C.

After the experiment was over the furnaces were switched off and the flow of reducing gas was stopped (in the case of second set of experiments). The inert gas was continued to flow for about 10 minutes.

After the reactor assembly was cooled down, the solid sample was taken out and chemically analyzed for degree of metallization. Gas samples collected during the second set of experiments were analyzed for percentage of hydrogen in the gas sample using the gas chromatograph employing molecular sieve column. An attenuation of 64X was used for all experiments and peaks of hydrogen were recorded. Using nitrogen and hydrogen gas mixture of known composition the chromatograph was calibrated before each run.

Gas samples collected in the first set of experiments could not be analyzed due to the non-availability of

RESULTS AND DISCUSSION

In the first set of experiments on reduction of hematite, coke was used as the reducing agent with nitrogen as the fluidizing gas, whereas in the second set hydrogen was the reducing agent and a mixture of hydrogen and nitrogen served as the fluidizing medium.

Reduction of Hematite with coke :

Variables studied in this set of experiments have been tabulated in Table 6.1. As the main objective of this part of investigation was to follow the kinetics of reduction reaction by continuous analysis of the outlet gas mixture using a chromatograph. However, as it has already been stated because of the problem within the chromotograph the analysis of the outgoing gases could not be carried out. This problem rendered the kinetics studies impossible. These experiments were, therefore, used only to check the workability of the FBR qualitatively. The only parameter that could be measured in this set of experiments was the weight of the sample after the experiment was over. This measurement did give some idea if of the extent of reduction of hematite under the given experimental conditions. Table 6.1 gives the final weights of the sample alongwith the weight loss. It can be seen that as expected the weight loss is greater at higher temperature and at the same temperature it is greater for finer particles.

Table No. 6.1: Experimental Conditions Explored for Reduction of Hematite Using Coke and Weight Loss Analysis

Sl. No.	Experiment No.	Temperature (°C)	Particle size (in mesh)		Initial weight of the sample (in gms)	Final weight of the sample (in gms)	Weight loss (in gms)
			Hematite	Coke			
1	EC1	850 ± 10°C	-72+100	-60+72	125	102.5	22.5
2	EC2	700 ± 10°C	-72+100	-60+72	125	110.5	14.5
3	EC3	700 ± 10°C	-100+150	-85+100	125	108.0	17.0
4	EC4	700 ± 10°C	-150+170	-100+120	125	100.5	24.5

Reduction of Hematite with Hydrogen

Experimental conditions employed in this set of experiments are tabulated in Table 6.2. In these experiments it could be possible to measure the composition of the outgoing gases. As on line analysis was not possible, gas samples were collected in specially designed gas sampler and could be analysed using a chromatograph. The outgoing gases would consists of nitrogen, hydrogen and water. However, at room temperature water could condense leaving nitrogen and hydrogen in the gas mixture. From this initial composition of the inlet gas and the analysis of the moisture free outlet gases, it could be possible to determine the amount of hydrogen consumed during the reaction as a function of time. This enabled us to compute the rate of formation of water. A typical plot giving percentage hydrogen in the outlet gas as a function of time is shown in Fig.6.3. Rate of hydrogen consumption as a function of time along with the rate of water formation and percentage oxygen removed in all the five experiments are given in Appendix III. Fig. 6.4 is a plot of percentage oxygen removed as a function of time for all the five experiments.

It should be noted that the rate of removal of oxygen in the initial stages of reduction is higher. It is attributed to the fact that the reduction of Fe_2O_3 to FeO with hydrogen at temperature employed in this study is thermodynamically much more favourable as compared to the reducti

Table No. 6.2 : Experimental Conditions Adopted for Reduction of Hematite Pellet Hydrogen and Weight Loss Analysis

Sl. No.	Experiment No.	Inlet Gas Composition	Temperature (^{o}C)	Particle Size (in mesh)	Initial weight of the sample (in gms)	Final weight of the sample (in gms)	Weight loss (in gms)
1	6	EH1	50 Percent H_2	800 ± 10	100	81.5	18.5
2	7	EH2	50 Percent H_2	700 ± 10	100	87.7	12.3
3	8	EH3	50 Percent H_2	750 ± 10	100	83.2	16.8
4	9	EH4	55 Percent H_2	750 ± 10	100	85.8	14.2
5	10	EH5	50 Percent H_2	700 ± 100	-72+100	100	83.5	16.5
6	11	EH6	50 Percent H_2	800 ± 10	100	77.5	22.5
7	12	EH7	23-25Percent H_2		100	92.7	7.3
8	13	EH8	25 Percent H_2	750 + 10	-100+150	100	91.2	8.8
9	14	EH9	30 Percent H_2		100	83.6	16.4

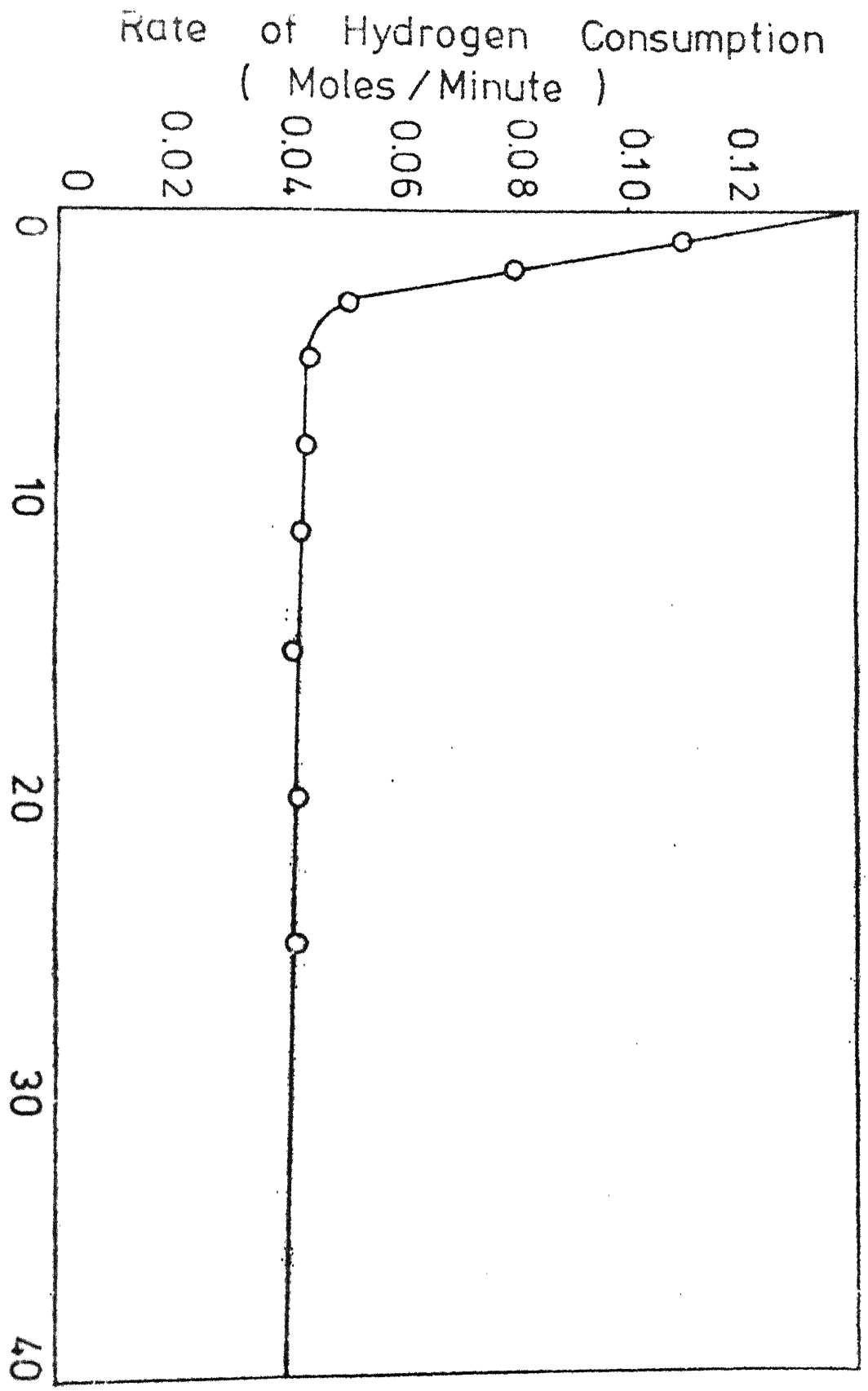

Figure 3. Rate of Hydrogen consumption

EH4
EH5
EH9
EH7
EH8
0.1
reduction.

of FeO to metallic iron. Also the presence of water vapours which are generated as a result of the reduction reaction tend to slower down the reduction reaction.

In this case also the sample was weighed after a particular experiment was over and this weight loss thus obtained was compared with that estimated from Fig. 6.4. It is observed that the estimated weight loss was higher in some cases than the actually measured weight loss. It is expected that during cooling of the sample inside the reactor before it could be taken out and weighted, some reoxidation took place which resulted in increased weight of the final sample.

As stated above also, the main purpose of these experiments was to test the workability of the high temperature FBR qualitative analysis of results at least indicate that this FBR may be used for more rigorous quantitative studies involving exothermic gas solid reactions.

CHAPTER - 7

SUMMARY AND CONCLUSION

It was proposed to design and fabricate a high temperature fluidized bed reactor which could be used to study the kinetics of endothermic gas-solid reactions in particular, the reduction of hematite with solid, solid and gas and gaseous reductants.

It was thought desirable to fabricate a cold model FBR before the fabrication of high temperature FBR was undertaken. Cold model FBR was used to test the fluidization characteristics for different operating variables such as distributor plate design, particle size, particle density, bed height etc. Visual observations in the cold model provided an added advantage which helped in detecting the possible malfunctioning of the fluidized bed. A number of experiments were carried out on cold model FBR to select the optimum operating conditions for the high temperature FBR.

The physical dimensions and the main design features in high temperature FBR were identical to those used in the cold model FBR. The main reactor and the gas preheater could be heated up independently of each other by providing two separate furnances. According to the original plan of the work the reduction of hematite with coke and methane

CHAPTER - 7

SUMMARY AND CONCLUSION

It was proposed to design and fabricate a high temperature fluidized bed reactor which could be used to study the kinetics of endothermic gas-solid reactions in particular, the reduction of hematite with solid, solid and gas and gaseous reductants.

It was thought desirable to fabricate a cold model FBR before the fabrication of high temperature FBR was undertaken. Cold model FBR was used to test the fluidization characteristics for different operating variables such as distributor plate design, particle size, particle density, bed height etc. Visual observations in the cold model provided an added advantage which helped in detecting the possible malfunctioning of the fluidized bed. A number of experiments were carried out on cold model FBR to select the optimum operating conditions for the high temperature FBR.

The physical dimensions and the main design features in high temperature FBR were identical to those used in the cold model FBR. The main reactor and the gas preheater could be heated up independently of each other by providing two separate furnances. According to the original plan of the work the reduction of hematite with coke and methane

was to be studied. As the methane gas was not readily available in market, it was decided to generate methane in the laboratory. Therefore, a setup for generating and storing methane was fabricated. However, this plan of the work had to be abandoned because of the problem with our chromatograph due to which online analysis of the out going gases could not carried out. A few high temperature experiments were, however, carried out to atleast qualitatively test the workability of the high temperature FBR. The experiments included reduction of hematite at temperatures between 700 - 800°C using coke, and hydrogen as the reductants.

In the case of reduction experiments involving hydrogen, the samples of out going gases were collected at regular interval of time in a specially designed gas sampler and analysed after each experiment. From the analysis of the initial and the final gas compositions it could be possible to estimate the extent of reaction in terms of percent oxygen removed as a function of time.

CONCLUSIONS:

Out of the three distributor plate design examined using the cold model FBR the one shown in Figure 4.1(D_1) was found to be most satisfactory for a larger range of operating variables. This design was, therefore, used for the high temperature FBR. Two of the other designs, which were discarded, gave a lot of channelling due to improper

gas distribution, which could be visually observed in the cold model FBR.

Minimum fludization velocities estimated using experimental plots of pressure drop versus velocity at different operating conditions were in close agreements with those obtained theoretically. Minimum fluidization velocity was found to increase with increasing density and particle size, larger bed heights. For bed consisting of fine particles affected the smooth fluidization behaviou due to the slugging.

Preliminary analysis of kinetic data on reduction of hematite with hydrogen indicated that the rate of reduction increased (i) with decreasing particle size (ii) with increased temperature and (iii) with increased partial pressure of the reducing gas. These observations, though trivial, clearly indicated the successful working of the FBR designed by us. With proper facilities for the analysis of the out going gas samples (preferably on line) the FBR can be used as one of very effective techniques of studying the kinetics of gas solid reactions.

APPENDIX I

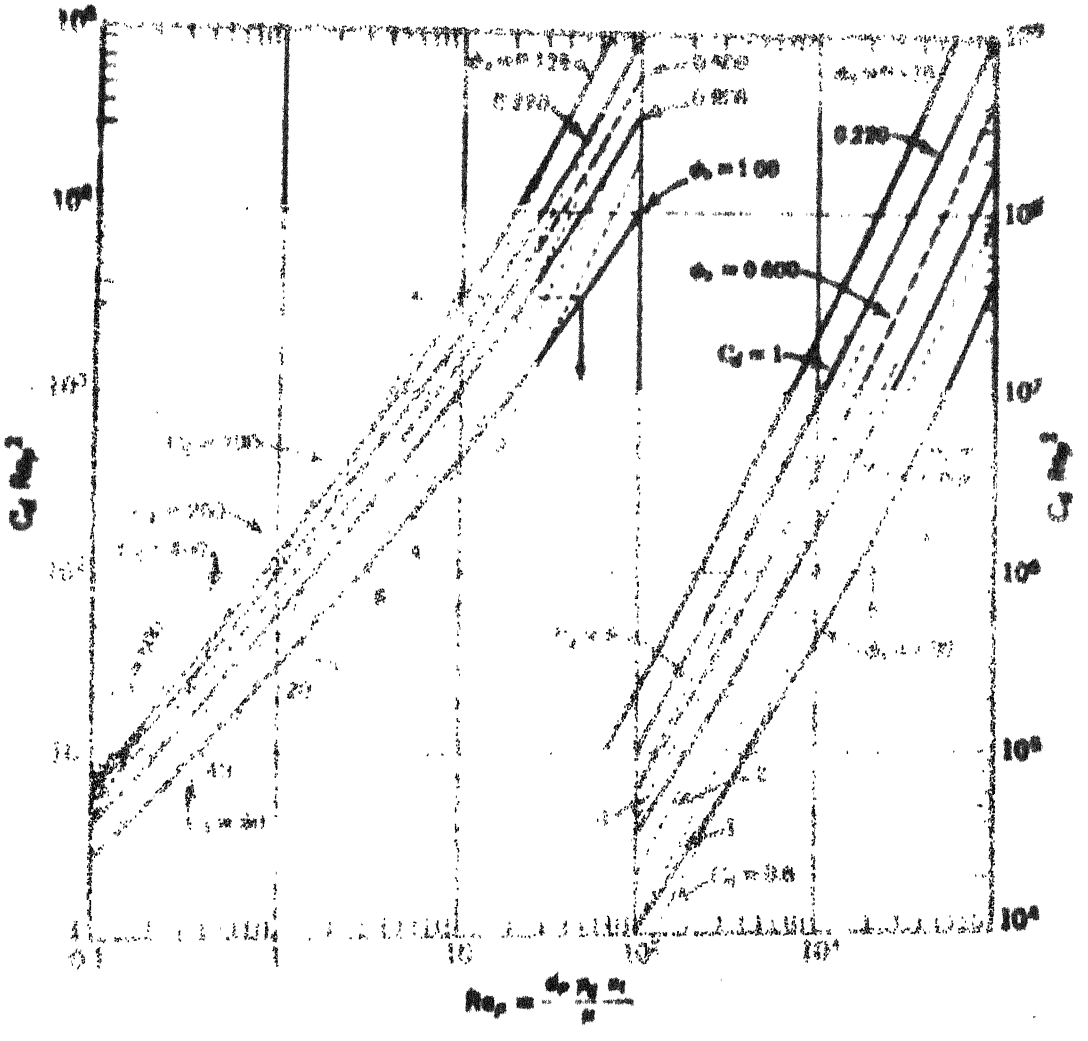

$C_d Re_p^2$ vs Re_p plot

(adapted from Kunii & Levenspiel (1))

APPENDIX II

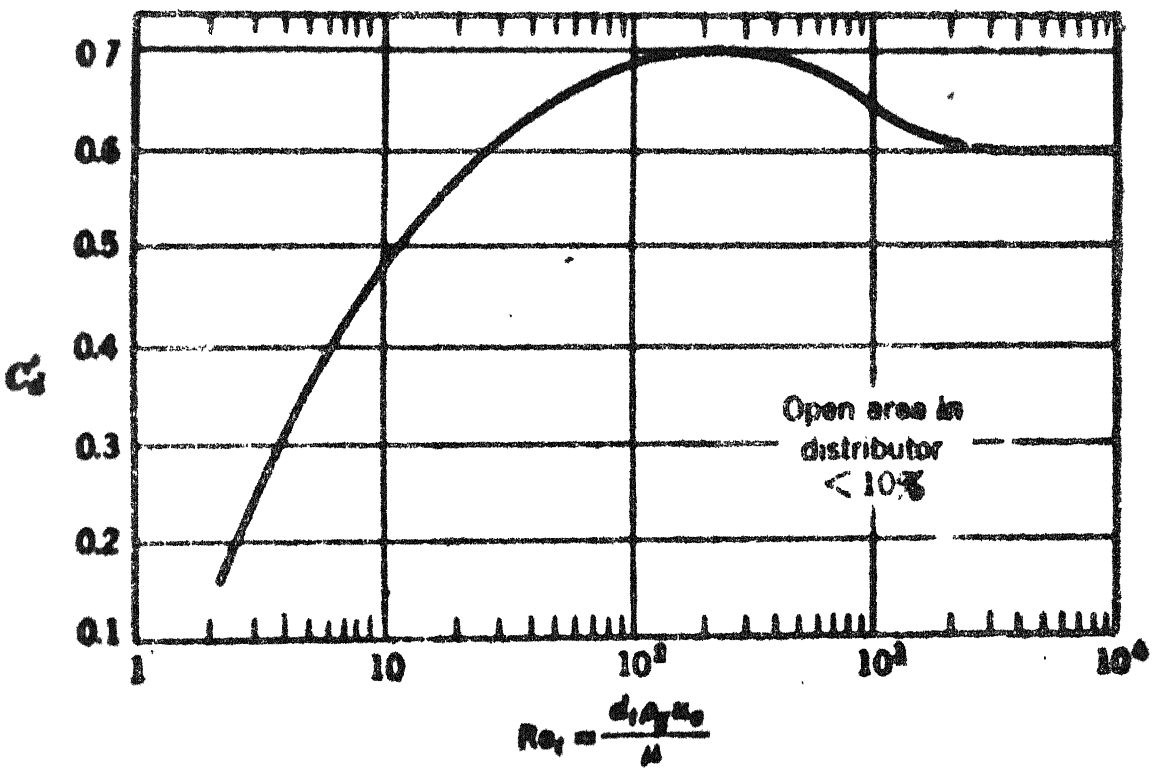

C_d' vs Re_p plot. (adapted from Perry (

Experiment EH 4

Flow rate of inlet gas: 6 lpm
Hydrogen : 55 o/o
Nitrogen : 45 o/o

Time (min)	X	Volume flow rate of Hydrogen in inlet gas (L/min)	Volume flow rate of Hydrogen in outlet gas (L/min)	Rate of Hydrogen consumption (L/min)	Rate of water formation (mole/min)	Cumulative amount of water formed (mole)	Percentage of oxygen removed (o/o)
2	0.200	3.3	0.675	2.625	0.1074	0.256	13.65
4	0.400	3.3	1.800	1.500	0.0613	0.435	23.20
7	0.475	3.3	2.443	0.857	0.0350	0.565	30.13
10	0.540	3.3	3.170	0.130	0.0053	0.655	34.93
15	0.490	3.3	2.594	0.706	0.0290	0.805	42.93
20	0.500	3.3	2.700	0.600	0.0245	0.939	50.08
25	0.500	3.3	2.700	0.600	0.0245	1.069	57.01
35	0.510	3.3	2.810	0.490	0.0200	1.293	68.96
40	0.520	3.3	2.810	0.375	0.0153	1.493	79.62

X - Fraction of Hydrogen in outgoing gases = $\frac{n_{H2}}{n_{H2} + n_{N2}}$

Initial weight of the hematite sample = 100 g.
Final weight of the reduced sample = 85.8 g.
Weight loss = 14.2 g.

Experiment EH 5

Flow rate of inlet gas: 6 lpm
Hydrogen : 50 %
Nitrogen : 50 %

Time (min)	X	Volume flow rate of Hydrogen in inlet gas. (L/min)	Volume flow rate of Hydrogen in outlet gas (L/min)	Rate of Hydrogen consumption. (L/min)	Rate of water formation (mole/min)	Cumulative amount of water formed (mole)	Percentage of oxygen removed (o/o)
1	0.11	3.0	0.371	2.629	0.108	0.1200	5.73
2	0.27	3.0	1.110	1.890	0.077	0.2125	9.86
3	0.37	3.0	1.762	1.238	0.051	0.2775	12.58
5	0.39	3.0	1.918	1.082	0.094	0.3705	14.88
8	0.39	3.0	1.918	1.082	0.044	0.5005	17.28
11	0.40	3.0	2.000	1.000	0.041	0.6305	19.47
15	0.40	3.0	2.000	1.000	0.041	0.8005	21.65
20	0.40	3.0	2.000	1.000	0.041	1.0105	23.84
25	0.41	3.0	2.000	1.000	0.041	1.2205	26.02

X - Fraction of Hydrogen in outgoing gas $= \frac{n_{H2}}{n_{H2} + n_{N2}}$

Initial weight of the hematite sample = 100 g
Final weight of the reduced sample = 83.5 g.
Weight loss = 16.5 g.

Experiment E7

Flow rate of inlet gas : 6 lpm
Hydrogen : 23 - 25 o/o
Nitrogen : 77 - 75 o/o

ne in)	X	Volume flow rate of Hydrogen in inlet gas (L/min)	Volume flow rate of Hydrogen in outlet gas (L/min)	Rate of Hydrogen consumption (L/min)	Rate of water formation (mole/min)	Cumulative amount of water formed (mole)	Percentage of oxygen removed (o/o)
	0.00	1.5	0.000	1.500	0.0610	0.061	3.25
!	0.00	1.5	0.000	1.500	0.0610	0.122	6.51
;	0.01	1.5	0.045	1.455	0.0590	0.182	9.65
;	0.10	1.5	0.500	1.000	0.0410	0.282	11.84
3	0.19	1.5	1.056	0.444	0.0182	0.362	12.80
1	0.24	1.5	1.421	0.078	0.0032	0.407	12.96
5	0.23	1.5	1.344	0.156	0.0064	0.449	13.33
0	0.23	1.5	1.344	0.156	0.0064	0.489	13.65
5	0.24	1.5	1.421	0.078	0.0032	0.524	13.87

(- Fraction of Hydrogen in outgoing gases = $\frac{n_{H2}}{n_{H2} + n_{N2}}$

Initial weight of the hematite sample = 100 g.
Final weight of the reduced sample = 92.7 g.
Weight Loss = 7.3 g.

Experiment EH 8

Flow rate of inlet gas : 6 lpm
Hydrogen : 25 o/o
Nitrogen : 75 o/o

me in)	X	Volume flow rate of Hydrogen in inlet gas (L/min)	Volume flow rate of Hydrogen in outlet gas (L/min)	Rate of Hydrogen consumption (L/min)	Rate of water formation (mole/min)	Cumulative amount of water formed (mole)	Percentage of oxygen removed (o/o)
1	0.00	1.5	0.000	1.500	0.061	0.061	3.20
2	0.00	1.5	0.000	1.500	0.061	0.122	6.40
3	0.00	1.5	0.000	1.500	0.061	0.183	9.76
5	0.11	1.5	0.556	0.944	0.039	0.283	11.84
8	0.20	1.5	1.125	0.375	0.015	0.363	12.64
11	0.22	1.5	1.269	0.231	0.009	0.393	13.12
15	0.21	1.5	1.196	0.304	0.012	0.441	13.76
20	0.21	1.5	1.196	0.304	0.012	0.501	14.40
25	0.21	1.5	1.196	0.304	0.012	0.561	15.04

X - Fraction of Hydrogen in outgoing gas = $\frac{n_{H2}}{n_{H2} + n_{N2}}$

Initial weight of the hematite sample = 100 g.
Final weight of the reduced sample = 91.2 g.
Weight loss = 8.8 g.

Experiment EH9

Flow rate of inlet gas : 6 lpm
Hydrogen : 30%
Nitrogen : 70%

Time (min)	X	Volume flow rate of hydrogen in Inlet gas (l/min)	Volume flow rate of hydrogen in Outlet gas (l/min)	Rate of hydrogen consumption (l/min)	Rate of water formed (mole/min)	Cumulative amount of water formed (mole)	Percentage of oxygen removed (%)
1	0	1.8	0	1.8	0.074	0.074	3.95
2	0.02	1.8	0.086	1.714	0.070	0.149	7.68
3	0.05	1.8	0.221	1.58	0.065	0.215	11.51
5	0.1	1.8	0.467	1.33	0.054	0.334	14.02
8	0.13	1.8	0.628	1.172	0.048	0.479	16.58
11	0.15	1.8	0.741	1.059	0.043	0.602	18.88
15	0.2	1.8	1.05	0.75	0.031	0.736	20.53
20	0.25	1.8	1.4	0.4	0.016	0.851	21.38
25	0.26	1.8	1.4	0.4	0.016	0.931	22.24

X - Fraction of Hydrogen with outgoing gas $= (n_{H_2})/(n_{H2}+n_{N2})$

Initial weight of the hematite sample = 100 g

Final weight " = 83.6 g

Weight loss " = 16.4 g

REFERENCES

1. "Fluidization Engineering", Daizo Kunii & Octave Levenspiel, John Wiley & Sons, Inc.

2. "Progress in Extractive Metallurgy", Vol. I, Fathi Habashi, Gorden & Breach Science Publishers, 21-93.

3. M. Leva, "Fluidization", McGraw-Hill Book Company, New York, 1959.

4. K. Natesan & W.O. Philbrook, Met.Trans., 1, May 1970, 1353-1360.

5. Y. Fukunaka et al, Met. Trans, 7B, Sept. 1976, 307-314.

6. H.A. Doheim et al, Met. Trans, 7B, Sept. 1976, 477-483.

7. F.M. Stephens, Chem. Engg. Progress, 49, No.9, 455-458.

8. Kondo et al, Australia Japan Extractive Metallurgy Symposium, 1980, 223-232.

9. J.W. Evans et al, Met. Trans 7B, Mar 1976, 55-65.

10. A.B. Michael & J.E. Hanway, Jr., J. Metals, 1964, 16, 881-884.

11. A.J. Morris & R.F. Jensen, Met. Trans. 7B, March 1976, 89-93.

12. A. Bergholm, Trans AIME, 1961, 221, 1121-1129.

13. L.A. Gutierrez & A.P. Watkinson, Fuel, 61, Feb. 1982, 133-

14. D.F. Othmer, "Fluidization", Reinhold Publishing Corp., New York, 1956.

15. Moosan Kwauk, Scientia Sinica, XXII, No.11, Nov.1979,

16. S. Yagi and D. Kunii, Chem. Engg. Sci., 1961, 16, 364-371.

17. ibid, 372-379.

18. ibid, 380-391.

19. A.R. Otero and R.C. Munoz, Powder Technology, 9(1974), 279-286.

20. D. Ghosh, M.Tech. Thesis, I.I.T. Kanpur.

21. J.H. Perry (Ed.) Chemical Engineers' Handbook, III Ed. McGraw-Hill Book Company, New York, 1963.